Copyright Warning & Restrictions

The copyright law of the United States (Title 17, United States Code) governs the making of photocopies or other reproductions of copyrighted material.

Under certain conditions specified in the law, libraries and archives are authorized to furnish a photocopy or other reproduction. One of these specified conditions is that the photocopy or reproduction is not to be "used for any purpose other than private study, scholarship, or research." If a, user makes a request for, or later uses, a photocopy or reproduction for purposes in excess of "fair use" that user may be liable for copyright infringement,

This institution reserves the right to refuse to accept a copying order if, in its judgment, fulfillment of the order would involve violation of copyright law.

Please Note: The author retains the copyright while the New Jersey Institute of Technology reserves the right to distribute this thesis or dissertation

Printing note: If you do not wish to print this page, then select "Pages from: first page # to: last page #" on the print dialog screen

ABSTRACT

A 3-DIMENSIONAL VASCULARIZED CARDIAC TISSUE MODEL USING CHITOSAN NANOFIBER SCAFFOLDS

by
Ali Hussain

The development of an in vitro tissue model that can mimic the 3-dimenisonal (3-D) cellular architecture and mosaic of myocardial tissue holds great value for cardiac tissue engineering, modeling, and cardiovascular drug screening applications. The main objective of this project was to develop a 3-D vascularized cardiac tissue model in vitro for improved survival and function.

The cellular mosaic of the myocardial tissue demands the intricate integration of an extracellular matrix-like scaffold, cellular constituents, and biological factors. The first aim of the research was to fabricate and characterize a biodegradable chitosan nanofiber scaffold that would resemble the extracellular matrix (ECM) physically and chemically. Chitosan, a natural polysaccharide that shares structural homology to the ECM glycosaminoglycans was processed into nanofibers via electrospinning to resemble the physical nano-architecture of the ECM. The second aim was to biologically modify the scaffold using a two step method: (1) Adsorption of fibronectin to improve cellular attachment and migration and (2) Induction of endothelial tubulogenesis to recreate the vascularized architecture of the myocardium. The third aim was to investigate the effect of co-culturing cardiomyocytes with fibroblasts on cardiomyocytes' survival and contractility in the vascularized 3-D chitosan scaffold. This was based on the fact that 70% of the native myocardial tissue is composed of fibroblasts.

The chitosan scaffold was characterized for its physio-chemical properties, including in-vitro structural integrity and bio-degradability. The biomodification of the scaffold via fibronectin adsorption improved cellular attachment, verified by staining of actin (cytoskeletal protein) and vinculin (cell-adhesion protein). The endothelial cells formed a network of interconnected tubes and secreted GAGs that were immobilized onto the chitosan scaffold. The cellular studies showed that cardiomyocyte mono-cultures resulted in islands of isolated contractions and minimal gap junction expression. In addition, cardiomyocyte contractility was lost after four days in the mono-cultures. However, co-culturing the cardiomyocytes with the fibroblasts promoted tissue-like synchronous contractions that were sustained for over three weeks. Gap junction expression in cardiomyocytes-fibroblasts co-cultures was extensive and was expressed along the cardiomyocyte cell membranes.

Finally, to create the cardiac tissue model, the vascularized chitosan nanofibers were impregnated with a co-culture system of cardiomyocytes and fibroblasts. Using real-time intracellular calcium ion staining, the cardiomyocytes were observed to have migrated through the 3-D chitosan scaffold and attained intercellular alignment to form cardiomyocyte tubules which is a characteristic of in vivo cardiomyocytes. The cardiomyocyte tubules were verified to contract in a synchronized and tissue-like rhythmic manner. These results highlight the immense importance of the vascular architecture and fibroblasts co-culture in the development of any cardiac regenerative therapy.

A 3-DIMENSIONAL VASCULARIZED CARDIAC TRI-CULTURE MODEL USING CHITOSAN NANOFIBER SCAFFOLDS

by
Ali Hussain

A Dissertation
Submitted to the Faculty of
New Jersey Institute of Technology
and University of Medicine and Dentistry of New Jersey
in Partial Fulfillment of the Requirements for the Degree of
Doctor of Philosophy in Biomedical Engineering

Department of Biomedical Engineering

May 2011

APPROVAL PAGE

A 3-DIMENSIONAL VASCULARIZED CARDIAC TRI-CULTURE MODEL USING CHITOSAN NANOFIBER SCAFFOLDS

Ali Hussain

Dr. Cheul Cho, Dissertation Co-Advisor Date
Assistant Professor of Biomedical Engineering, NJIT

Dr. George Collins, Dissertation Co-Advisor
Date
Research Professor of Biomedical Engineering, NJIT

Dr. William Hunter, Committee Member Date
Professor of Biomedical Engineering, NJIT

Dr. Treena Arinzeh, Committee Member Date
Associate Professor of Biomedical Engineering, NJIT

Dr. Pranela Rameshwar, Committee Member
Date
Professor of Medicine, University of Medicine and Dentistry of New Jersey
New Jersey Medical School

Dr. Diego Fraidenraich, Committee Member
Date
Assistant Professor of Cell Biology, University of Medicine and Dentistry of New Jersey
New Jersey Medical School

BIOGRAPHICAL SKETCH

Author: Ali Hussain

Degree: Doctor of Philosophy

Date: May, 2011

Undergraduate and Graduate Education:

- Doctor of Philosophy in Biomedical Engineering,
  New Jersey Institute of Technology, Newark, NJ, 2011

- Master of Science in Biomedical Engineering,
  New Jersey Institute of Technology, Newark, NJ, 2008

- Bachelor of Science in Biology,
  University of Toledo, Toledo, OH, 2006

Major: Biomedical Engineering

Presentations and Publications:

Peer-Reviewed Articles

Hussain, A., Chou, S. Pelletier, M. (2011) Characterizing the behavior of Single Walled Carbon Nanotubes (SWNTs) using Raman spectroscopy in a crystallized system: A step toward designing SWNT stress probes. *The Journal of Pharmaceutical Sciences* (in preparation).

Hussain, A., Collins, G., Cho, C. (2011) 3-D vascularization of electrospun chitosan: novel tube formation technique. *Acta Biomaterialia* (in preparation).

Shalaev, E., Soper, A., Chou, S., Pikal, M., Luthra, S., Hong, J., Ewing, S., Collins, G., Hussain, A., Fitch, A., Sztucki, M., Narayanan, T., Bates, S. (2011) Water distribution in carbohydrate glasses: implications for solid-state stability of amorphous pharmaceutical solids. *Journal of Pharmaceutical Sciences* (in preparation).

Hussain, A., Collins, G., Cho, C. (2011) Characterization of electrospun chitosan scaffolds and their in vitro cytocompatibility. *Biomaterials* (in preparation).

Hussain, A., Collins, G., Cho, C. (2010) Functional 3-D Cardiac Co-Culture Model Using Fibronectin-Coated Chitosan Nanofiber Scaffolds. *Tissue Engineering* (submitted).

Hussain, A., Collins, G., Cho, C. (2010) Electrospun chitosan-based nanofiber scaffolds for cardiac tissue engineering applications., Proceedings of 2010 IEEE (26): 1-2.

Poster presentations

Hussain, A., Collins, G., Cho, C. (2010) The development and characterization of bioinspired chitosan electrospun nanofibers for tissue engineering applications. NJIT Graduate Student Association Research Day, Newark, NJ.

Hussain, A., Collins, G., Cho, C. (2010) Electrospun chitosan-based nanofiber scaffolds for cardiac tissue engineering applications. 36th Northeast Bioengineering Conference, New York, NY.

Shalaev, E., Soper, A., Chou, S., Pikal, M., Luthra, S., Hong, J., Ewing, S., Collins, G., Hussain, A., Fitch, A., Sztucki, M., Narayanan, T., Bates, S. (2010) Water distribution in carbohydrate glasses: implications for solid-state stability of amorphous pharmaceutical solids. 11th International Symposium on the Properties of Water. Queretaro, Mexico.

Ewing, S., Hussain, A., Collins, G., Fitch, A., Bates, S., Sztucki, M., Narayanan, T., Shah P., Roberts, C., Chou, S., Shalaev, E., (2009) Water distribution in concentrated sugar solutions: "water clusters" vs "3-dimensional network" models. 31st International Conference on Solution Chemistry. Innsbruck, Austria.

Hussain, A., Collins, G., Cho, C. (2009) Electropsun Chitosan-Based Nanofiber Scaffolds for Cardiac Tissue Engineering Applications. NJIT Graduate Student Association Research Day, Newark, NJ.

Book Chapter

Shalaev, E., Collins, G., Hussain, A., Ewing, S., Roberts, C. (2011) Mobility of water in sugar glasses: thermally stimulated current study (in preparation).

Provisional Patent Filed

Hussain, A., Cho, C., Collins, G. System and Method for Vascularized Biomimetic 3-D Tissue Models. U.S. Provisional Patent No. 61/448483.

(In the Name of God, the Most Merciful, the Most Forgiving)

(Calligraphy by Hassan Musa)

I was born into this world with no say of mine,

I will leave this world regardless of my choice of time.

I have made mistakes, for those I apologize,

Accomplishments and successes, those I don't prize.

But I share them with every person that happened,

To guide my caravan to the oasis more enlightened.

By Ali Husain

I dedicate my thesis to my father and my mother, both of whom couldn't complete their education

Because life had other plans for them.

I dedicate my thesis to my beautiful wife, Horia.

I dedicate my thesis to my twins, Baby A and Baby B.

ACKNOWLEDGEMENT

I would like to express my deepest gratitude and appreciation to Dr. Cheul Cho. Thank you for teaching, supporting, and letting me grow in your lab. I would like to immensely thank Dr. George Collins for being THE BEST mentor, guide, and above all a friend. Thank you both for very believing in me.

I would like to thank Dr. William Hunter and Dr. Treena Arinzeh from NJIT and Dr. Pranela Rameshwar and Dr. Deigo Fraidenraich from UMDNJ for being part of my PhD dissertation committee. I would like to thank Dr. Junichi Sadoshima and Dr. Haesun Kim for the gift of neonatal cardiomyocytes and pups. I would like to thank the Medical Device Concept Laboratory (MDCL) and Material Characterization Laboratory (MCL) for allowing me to conduct my experiments using their equipments. I would like to thank Dr. Zohar Ophir for his help during electrospinning and Dr. John Suwardie for his rheology expertise. I would like to thank Dr. Xueyan Zhang for training me to use the SEM. I would like to thank Dr. Jeong Shim for teaching me how to use the XRD machine and analyze its data. I would like to thank Dr. Lai-Hua Xie for his immense help in performing the intracellular calcium ion staining and teaching me how to perform the flux studies. I would like to thank the Biomedical Engineering Department for support me during my research and the NJIT startup fund for supporting my work.

I would like to thank my lab mates (previous and current) and the entire Biomedical Engineering department for their constant support and encouragement.

I would like to thank my wife who was very patient as I disappeared for long stretches of time in the lab.

Thank you all.

TABLE OF CONTENTS

TABLE OF CONTENTS
(Continued)

TABLE OF CONTENTS
(Continued)

Chapter **Page**

TABLE OF CONTENTS
(Continued)

Chapter **Page**

LIST OF TABLES

LIST OF FIGURES

LIST OF FIGURES
(Continued)

LIST OF FIGURES
(Continued)

LIST OF FIGURES
(Continued)

LIST OF FIGURES
(Continued)

CHAPTER 1

INTRODUCTION

1.1 Tissue Engineering

Tissue engineering was born out of the need to replace organs or tissues that become incompetent due to age, trauma, or pathologies. Some organs such as the heart and brain do not possess extensive regeneration capabilities following major trauma. Organ transplantation has been the main solution for complete organ failures. However, organ transplantation comes with a number of major drawbacks such as donor shortage, immuno-rejection and risk of transferring donor cancer stem cells. Other organ and tissue replacement approaches involve autografts (transplanted from the patient's own healthy tissue), allografts (transplanted from a genetically non-identical member of the same species), and biomaterial medical device implants. These tissue replacement methods have disadvantages which include donor site morbidity, poor integration, and immunologic reactions.

Tissue engineering has emerged as an alternative option to organ transplantation and replacement since it presents the opportunity to provide "off the shelf" and immunologically safe tissue regenerative solutions that help the body heal itself. Advances in tissue engineering have accelerated due to interdisciplinary collaboration between researchers in biology, medicine, material science, and engineering. The advancement and maturity of tissue engineering as a field depends on the extent of this interdisciplinary integration, since understanding tissue-specific functionality and repair mechanism is a very complex process. Furthermore, every tissue is unique in its cellular

composition and architecture, physiological requirements, extracellular niche, and many other biological, physical, and chemical parameters. Figure 1.1 illustrates the key factors that are involved in designing and developing a tissue engineered construct.

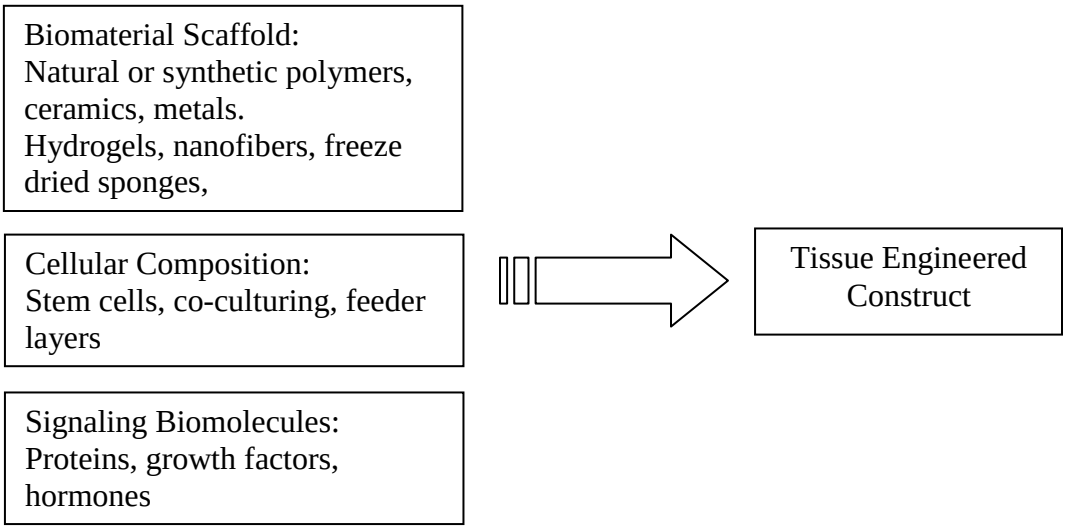

Figure 1.1 The main components of a tissue engineered construct.

1.2 Myocardial Infarction and Cardiac Tissue Engineering

Heart disease is a preeminent cause of death in the world, responsible for about 40% of human mortality. Annually in the United States, 550,000 new cases are diagnosed and about $33 billion is spent on dealing with heart failure [1]. There is a large variety of pathologies that cause heart failure such as ischemic heart disease which is sometimes accompanied with acute myocardial infarction, hypertension, and primary myocardial disease. Ischemic heart disease followed by an episode of acute myocardial infarction is the most frequent cause of left-sided cardiac failure [1].

One of the major causes of end stage heart failure is myocardial infarction. When the blood vessels supplying the physiologically demanding myocardium tissue become

occluded, the downstream tissue experiences ischemia. The metabolic strain on the myocardial tissue will lead to cardiomyocyte demise which is medically labeled as myocardial infarction. More importantly myocardial infarction leads to myocyte slippage. The term myocytes slippage refers to the sliding of bundles or singular myocytes along the longitudinal axis of the tissue lamina [2]. The necrosis of the cardiomyocytes caused by the ischemia activates multiple neurohormonal and inflammatory pathways, depicted in Figure 1.2, that lead to the degradation of the fibrillar collagen network connections that provide the structural integrity to the myocytes bundles.

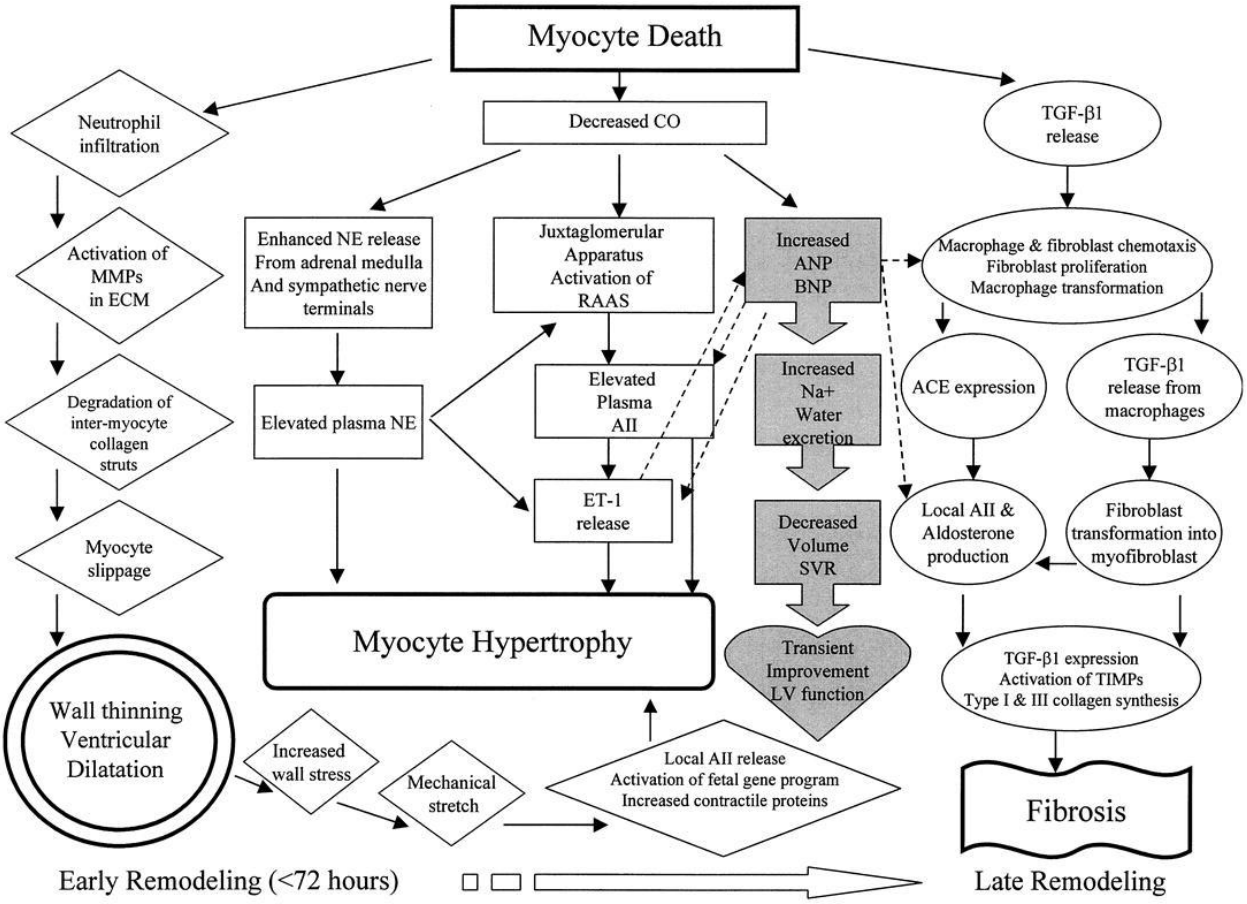

Figure 1.2 Flowchart representations of the pathophysiological events that develop during ventricular remodeling. ECM: extracellular matrix; RAAS: rennin-angiotensin-aldosterone system; CO: cardiac output; SVR: system vascular resistance; LV: left ventricle; and AII: angiotensin II. [3]

The replacement of the damaged myocardium with a non-contractile fibrous scar tissue compromises heart contractile efficiency. In addition, the collagenous extracellular matrix is weakened leading to a thin heart wall, ventricular dilation and remodeling. The damage to the heart wall is permanent because following extensive cell loss, the myocardium does not possess intrinsic regenerative capability [4]. Furthermore, the myocardium contains very limited and sparse number of cardiac stem cells making native regeneration a localized and ineffective solution for a large infracted region [5].

The ventricular remodeling that occurs following myocardial infarction is characterized by increase in cardiomyocyte cell volume: myocytes hypertrophy and the excess deposition of collagen fibers in the myocardial extracellular environment. These physiological and physical changes in the cellular and acellular components of the myocardium serve to compensate for the non-contractile scar tissue formed in the infarcted heart. However, this excessive and pathological secretion of ECM components, mainly collagen, leads to systolic and diastolic dysfunction of the ventricles since it affects cardiac conduction capabilities [6]. As a result, the remodeled heart undergoes hypertrophy and increased collagen secretion that eventually predisposes it to end stage of congestive heart failure.

Currently, several medical treatment regiments are indicated to control the ventricle remodeling or slow the pace of progression to heart failure. Pharmacological therapeutics reduces the heart's work load via diuretics and nitrates. In addition, humoral factors can be blocked, via ACE inhibitors or B-blockers, since they are over activated in heart failure [7]. Interventional therapy, such as implanting pacing devices can be performed to control electrical/mechanical asynchrony. Nonetheless, pharmaceutics and

surgery fall short from preventing progression to end stage heart failure [8]. Ultimately, heart transplantation is the final option for end-stage heart failure. However, due to the scarcity of heart donors and the confines and complications linked with immune suppression and rejection researchers are turning towards cardiac tissue engineering to discover effective solutions to revive the distressed heart.

Seminal studies published in the early 1990s depicted long-term survival and differentiated phenotype of transplanted skeletal myoblasts in the ventricular myocardium [9-11]. These studies paved the way for cardiac tissue engineering and shed light on the possibility of replacing the injured myocardium with healthy cells. Cell transplantation procedures into the injury site are dependent on the cell species and the transplantation method to provide optimal engraftment of the cells. Every cell in the body requires a niche which is characterized by unique physical, chemical, and biological parameters that supports its survival and induces optimal cellular functionality. It has been reported that more than 90% of the cells injected into the ventricular wall are lost since the cells do not undergo engraftment immediately when introduced into the native heart tissue [12].

Hence, the goal of in vitro myocardial tissue engineering, as seen in Figure 1.3, is to create a physically, chemically, and biologically designed scaffold that the cells can adhere to and function on, until they engraft within the native tissue. The ex vivo generation of a 3D myocardial tissue employing cells, biomaterials, and bio-molecules provides a temporary niche for the cardiomyocytes to become functionally mature and improve the chances of engraftment post-implantation.

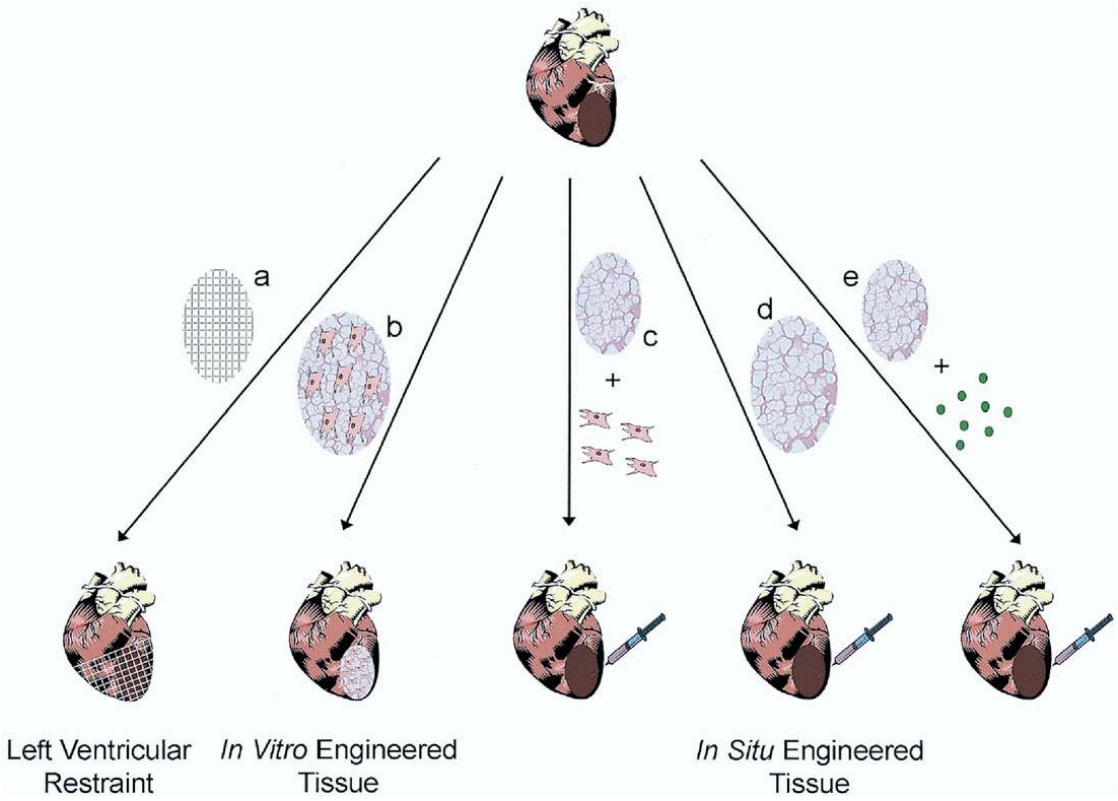

Figure 1.3 Potential tissue engineering methods for the treatment of myocardial infarction. (1) Polymer restraints can be used to maintain the left ventricles geometry and slow ventricular remodeling. (2) In vitro tissue engineering utilizes biomaterial scaffolds impregnated with cells in vitro and then transferred to the epicardial infarcted region. (3) In situ tissue engineered involves the local injection of a biomaterial, or biomaterial + cells or only biological factors. [13]

1.3 Current State of the Art

The objective of cardiomyocyte-based engineered tissue constructs is to produce a contractile tissue-like patch that can be used to restore the contractility and pumping efficiency of the infracted region. Ideally, these constructs have to be clinically relevant in terms of thickness (~1.5cm for human myocardium), mechanical stiffness (10-20 kPa at the start of diastole and 200-500 kPa at the end of systole), and high cell density (2 x 10^8 cells/cm^3) consisting of aligned myofibers [14-17]. None of the cardiac constructs

currently generated have reproduced fully clinically relevant constructs in terms of thickness or functionality. The following are some promising examples of in vitro cardiac constructs that have been implanted in vivo.

Zimmerman et al. fabricated a ring-shaped cardiac construct using neonatal cardiomyocytes seeded on collagen I gel mechanically conditioned using a bioreactor. The construct exhibited spontaneous contractions and was shown to improve cardiac performance after implantation [18, 19]. However, the construct was 1-4mm thick and histological integration (desmosomes and gap junctions) between the implant and the host tissue was not confirmed.

Leor et al. developed cardiac grafts by culturing cardiomyocytes on freeze-dried alginate scaffolds and implanted them into the infracted myocardium. The observations demonstrated a significant increase in angiogenesis of the graft but no change in cardiac contractility [20]. Okano et al. produced cardiomyocyte cell sheets by culturing them on thermosensitive polymer poly (N-isopropylacrylamide). These polymers are hydrophobic and cell adhesive at 37°C; however, when the temperature is dropped to 32°C, they hydrate and become hydrophilic causing the cells to detach as a single cellular sheet [21]. These cellular sheets have been shown to electrically couple and pulse in a synchronized manner. In addition, four sheets were layered to form a pulsatile cardiac tissue grafts that was then implanted subcutaneously into rats and shown to survive three months in vivo [22]. Most of the developed cardiac constructs use only cardiomyocytes seeded on a biomaterial to implant in the infraction site.

1.4 Biomaterials

In my opinion, the main requirements for a biomaterial are biological performance and biodegradability. The author defines biological performance as the materials' ability to elicit the cells to perform the desired function without any adverse side-effects. An example of an adverse side-effect is inflammatory responses, the biomaterial must be a non-foreign body-reaction forming substance, i.e., its presence in the body should not trigger an immune response wherein macrophages start to fuse together forming foreign body giant cells that encapsulate the biomaterial and prevent it from performing its intended function [23]. Biodegradability defines the material's decomposition via natural in vivo processes. The degradation by products should be non-toxic and easily removed from the body.

Typically, biomaterials can be divided into two broad categories: natural and synthetic materials. Both categories have with advantages and disadvantages. Proteins are great natural materials since they possess the ability to exhibit receptor-binding amino acid sequences to the cells. They are also susceptible to cell-mediated proteolytic biodegradation. However, they have complex purification procedures and present the risk of disease transmission [24]. On the other hand, biologically inert and non-biodegradable synthetic materials provide batch-to-batch uniformity and can have manufactured tailored properties.

The choice and modification of the biomaterial is dependent on the intended application. For tissue engineering, each tissue or cell type will require certain chemical and physical requirements from the biomaterial to enable the optimum functioning of the engineered graft. The effect of the biomaterials on cellular function is a vital aspect in

ensuring that the cells can function when transplanted to the site of injury. For instance, nerve cells have been shown to exhibit significant enhancement in neurite extension when cultured on piezoelectric biomaterials [25, 26]. These piezoelectric biomaterials such as poled polyvinylidene fluoride contain transient surface charges that have been attributed to the improvement in neurite growth [27]. Similarly, skin regeneration is improved by the use of an upper silicone membrane which maintains a certain moisture level at the wound site, accelerating the healing process and induces skin re-growth [28].

1.4.1 Chitosan

Chitosan is a copolymer consisting of D-glucosamine and N-acetyl-D-glucosamine monomers derived from natural chitin by basic deacetylation. Because of chitosan's solubility in acidic solutions, it is used in more applications compared to chitin [29]. Recently chitosan's biodegradability, non-toxicity, wound-healing properties, biocompatibility, antimicrobial activity, and low immunogenicity have highlighted its potential in numerous industries ranging from waste-management, cosmetics, pharmaceutics, medicine and textiles [30-32]. Chitosan's use as a biomaterial is driven by its (1) economic cost (2) structural homology to the ECM GAGs as seen in Figure 1.4 (3) positive charge allowing it to interact with negatively charged GAGs and growth factors (4) anti-microbial properties and (5) derivation from chitin, the second most abundant natural polymer [33].

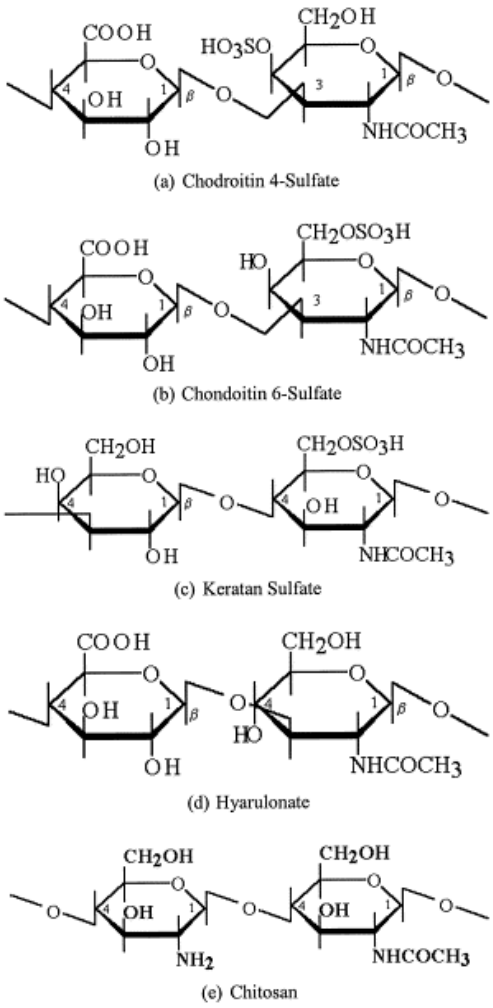

Figure 1.4 The structural homology of the natural glucosaminoglycans (a through d) to chitosan (e) [34]

In terms of tissue engineering applications, chitosan has been used in skin [35], bone [36], and neural [37]. To date, chitosan has not been used in cardiac tissue engineering as seen in Table 1.1 which is referenced from a 2010 published review on myocardial tissue engineering [38].

Table 1.1 List of Biomaterials Used in Cardiac Tissue Engineering

Materials	References
Natural materials	
Gelatin	[39]
Matrigel	[40]
Collagen	[41]
Alginate	[20]
Fibrin glue	[42]
Collagen and Matrigel	[43, 44]
Synthetic materials	
Polyglycolic acid (PGA)	[45, 46]
Poly(glycerol sebacate) PGS	[47]
Poly(e-caprolactone-co-L-lactide) (PCLA)	[48]
Poly(N-isopropylacrylamide) (PIPAAm)	[22]
Polyurethanes (PU)	[49]
Poly(glycolide-co-lactide) (PLGA)	[50]
PGA-co-poly-4-hydroxybutyrate (PGA/P4HB)	[51]

1.4.2 Scaffolds

Scaffolds provide a 3-dimensional physical structure where the cells can attach, migrate, generate their own extracellular matrix, and proliferate into a functional tissue according to the scaffold's shape. During the early 1980s, Bissell et al. published a groundbreaking report coining the term "dynamic reciprocity" to articulate the delicate interplay between the extracellular matrix's physical and chemical cues on the cell's cytoskeleton, nuclear matrix and ultimately gene expression [52]. Hence, the scaffold's design in terms of architecture and the biological performance is critical to the survival and optimum cellular functionality as seen in Figure 1.5. The scaffold also provides structural stability for the newly forming and developing tissue until it is capable of functioning in its native extracellular matrix.

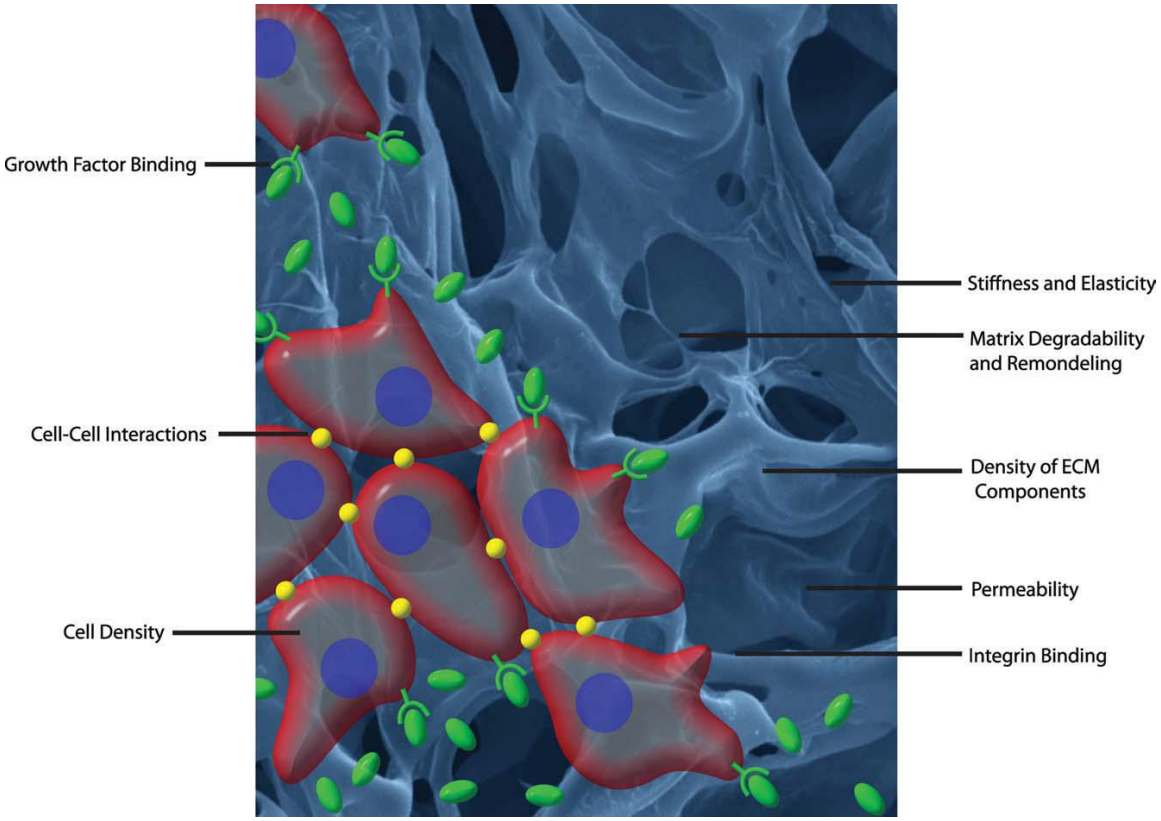

Figure 1.5 Graphical representation of a 3D biomaterial cellular scaffold portrays the signals that can be transferred to the cells via the physical architecture or biological components that ultimately control cell fate and functionality. The architectural components include but are not limited to the permeability, stiffness, degradability, and dimensionality of the structure. The biological components refer to proteins, growth factors or other bioresponsive molecules (molecules that elicit biological responses from cells) that can be incorporated within the scaffold to induce or activate certain molecular pathways. [53]

The best scaffold for the cells is the natural extracellular matrix generated by the cells themselves. Thus it comes as no surprise the extensive attention given to replicating the architecture and biological conductance of the natural extracellular matrix. The natural extracellular matrix can be divided into two main categories: interstitial/stromal and basement membrane [54]. Each type is unique in its architecture and biological composition. The interstitial extracellular matrix provides the intercellular milieu,

however the basement membrane is a sheet-like basolateral substratum that delineates cellular structures.

The architectural elements of the extracellular matrix include a network of fibrous protein components including collagen, fibrin, and elastin and a hydrogel matrix of glycosamino glycans such as hyaluronic acid, heparin sulfate, and keratin sulfate. Hence, the extracellular matrix can be visualized as a fiber reinforced hydrogel. The biological functionality of the extracellular matrix arises from its:

1. Ability to sequester, store, and present soluble growth factors and regulatory molecules [55].
2. Availability of multidomain proteins such as fibronectin, laminin, vitronectin, and entactin. These proteins have numerous functions such as cell attachment, activation of developmental processes, and cell differentiation [56].
3. Control of cell shape and cytoskeletal mechanics by changing the extracellular matrix stiffness [57].

Combining the architectural and biological aspects of the cell-extracellular matrix interaction, it is evident that a coupling between the insoluble architectural ECM factors and the chemical and biological soluble ECM factors tightly control the cells fate, survival, migration, proliferation, and differentiation [58].Furthermore, each tissue's ECM will vary significantly in terms of composition, physical structure, and biological components according to the developmental, functional, and healing processes. It is important to realize the function of the malleability of the ECM in response to physiological needs. For example, during cardiogenesis, the acellular ECM is surrounded by endocardial and myocardial cell layers. The endothelial cells differentiate into primordial heart valves in response to an increase in ECM synthesis by the myocytes. The primitive mouse ECM has been shown to retain bone morphogenic proteins and other transforming growth factor-beta family of cytokines in an inactive form until

activation is triggered by ECM degradation which induces endothelial cell migration and the advancement of cardiac development [59]. On the other hand, an increase in synthesis by fibroblasts during cardiac injury causes excess collagen deposition and fibrosis [60]. Hence, since the optimal scaffold for the cells is their native extracellular matrix; the engineered scaffold should interact with the natural extracellular matrix and enable the presentation of the ECM to the cells until complete engraftment in the host tissue.

1.5 Cell Sourcing

The biggest hurdle in cardiac tissue engineering is the quest for an appropriate cell source. The heart tissue is one of the most densely populated tissues, 40 million cardiomyocytes per gram of native myocardium [61]. Hence, the primary cells currently used in cardiac tissue engineering research are proof-of-concept substitutes. Cardiac tissue engineering cannot be translated into a clinically relevant therapy until an appropriate cell source has been found.

The following options are some of the cell sources currently being investigated for cardiac regenerative therapies:

1. Adult stem cells found in the bone marrow [62], peripheral blood [63], umbilical cord [64] and adipose tissue [65] have been observed to give rise to cardiomyocytes.
2. Resident progenitor cells in the heart have the potential to differentiate into functional cardiomyocytes [66].
3. Alternative to adult stem cells, embryonic stem cells have been shown to spontaneously differentiate into cardiomyocytes [67], however the major drawback of embryonic stem cells is their potential to form tumors and difficulty to differentiate into pure cell lineages.

The cell sourcing issue in cardiac tissue engineering remains to be the main determining factor on whether adult cardiac regeneration ever becomes a reality. Table

1.2 provides up to date cell sources that are currently being investigated to populate the injured heart.

Table 1.2 Review of the Cell Sources Used in the Treatment of Myocardial Diseases

Cell source	Differentiation potential	Current usage
Skeletal myoblasts	Terminal differentiation	Repopulate scar tissue and improve LV function
Marrow mesenchymal stem cells	Cardiomyocytes, vascular endothelium	Repopulate damaged myocardium
Bone marrow cells	Cardiomyocytes, vascular endothelium	Repopulate damaged myocardium
Endothelial progenitor cells	Vascular endothelium	Neo-vascularization to prevent myocardium apoptosis and LV remodeling
Resident cardiac stem cells	Cardiomyocytes	Improve cardiovascular function
Embryonic stem cells	Pluripotency	Revascularization and regenerate damaged myocardium
Induced pluripotent stem cells	Pluripotent	Repair damaged heart

Source: [38]

1.6 Objectives

This research's overall aim is to engineer a myocardial tissue model construct that can mimic the 3-dimensional cellular architecture and mosaic of myocardial tissue. This cardiac tissue model can potentially be used in myocardial tissue regeneration or utilized as a platform technology for diagnostics, drug screening or therapeutics. **The motivation is to attain extended cardiomyocyte viability and functionality in a 3-dimensional in vitro tissue model.** This study hypothesizes that co-culturing primary cardiomyocytes with fibroblasts will improve cardiomyocyte longevity and functionality in vitro. Specific aims are listed below:

1. The fabrication and characterization of chitosan nanofibrous scaffolds.

2. Biomodification of the chitosan nanofibrous scaffolds to create a vascularized cellular niche.

3. Improve cardiomyocyte longevity and functionality by co-culturing with fibroblasts. Impregnate the biomodified chitosan scaffolds with cardiomyocytes and fibroblasts co-culture and assess cardiomyocyte functionality.

The uniqueness of the approach taken in this research is the use of all three of the main cell types present in the myocardium: cardiomyocytes, fibroblasts, and endothelial cells to recreate the in vivo myocardial cellular niche. Moreover, the three cells types are not simply seeded on the scaffold, rather the scaffold will first be vascularized using endothelial cells to recreate the rich vasculature bed that perfuses the myocardial tissue and then the vascularized scaffold will be impregnated with a co-culture of cardiomyocytes and fibroblasts.

The novelties in this research are:

1. This is the first report to investigate the potential of chitosan nanofibers in the field of cardiac tissue regeneration.

2. This is the first report to induce vascularization on chitosan nanofibers. (*provisional patent filed*)

CHAPTER 2

FABRICATION AND CHARACTERIZATION OF ELECTROSPUN CHITOSAN SCAFFOLDS

2.1 Introduction to Electrospinning Chitosan

Electrospinning is a polymer processing technique that generates fibers in the micro- to nano-dimensions. Nanofiber scaffolds have are widely used in tissue engineering because of their architectural resemblance to the natural extra-cellular matrix. Furthermore, electrospinning provides a quick cost-effective and relatively simple processing method to produce ultra-fine nanofibers into non-woven oriented or non-oriented matrices. A typical electrospinning setup includes a metal needle connected to a syringe, a pump flow rate controller, a DC voltage supply and a grounded plate collector as shown in Figure 2.1

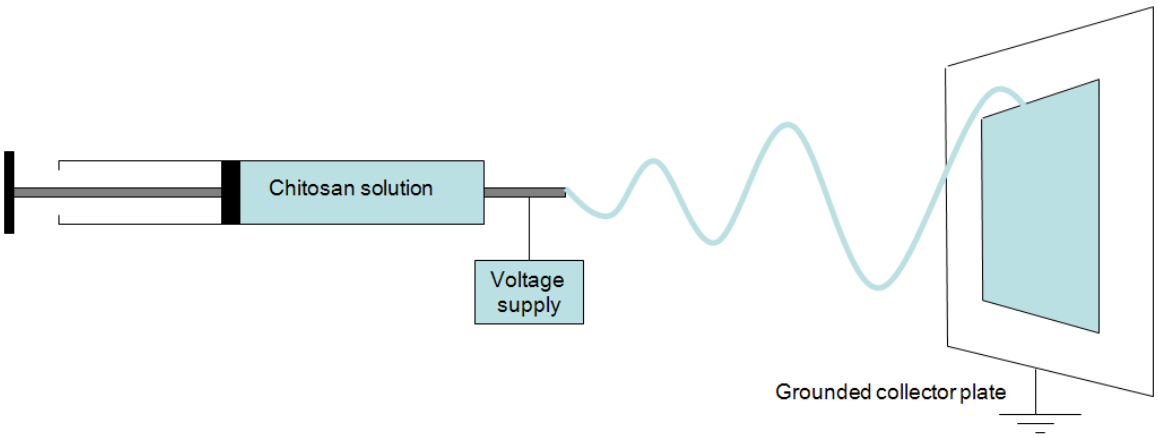

Figure 2.1 A typical electrospinning setup for the fabrication of a non-woven randomly oriented fiber matrix.

The theory behind the electrospinning process is that fiber formation occurs when the electrostatic forces created between the metal needle and the grounded collector plate has overcome the surface tension of the polymer solution. As the intensity of the

electrostatic forces increase, the polymer solution at the tip of the needle will elongate to form a Taylor cone. When the electrostatic forces overcomes the surface tension, the polymer solution gets drawn out as a taylor cone from which a linear region extends and undergoes a whipping process wherein the solvent evaporates very quickly depositing nano- to micro-scale fibers on the metal collector. There are many factors that affect the formation of electrospun fibers: (1) Solution properties: molecular weight or concentration which affects viscosity, electrical conductivity, polarity and surface tension of solution. (2) Electrospinning chamber properties: Voltage supply intensity, electrospinning distance, solution flow rate, humidity, and temperature [68].

The first published reports on electrospinning of pure chitin and chitosan were performed by Min *et al.* and Ohkawa *et al.* respectively in 2004 [69, 70]. Chitosan becomes water-soluble in acidic pH <6 by the protonation of the amine on the glucosamine group; this cationic nature poses a major challenge in electrospinning. Due to chitosan's polyelectrolyte behavior, hydrophilic nature, and water retaining properties; chitosan has the spontaneous capability to form gels in acidic pH which increases its viscosity and hinders the electrospinning process [71]. To overcome this challenge, high concentrations (80% to 100% v/v) of acids are usually used to electrospin chitosan ranging from moderately weak acids such as acetic acid to trifluoroacetic acid [69, 72, 73].

This section of the research focused on the fabrication of the chitosan nanofibers and their physical, chemical, and thermal material analytical characterization.

2.2 Methods

2.2.1 Rheological Measurements of Chitosan Electrospinning Solution

Commercially available medium molecular weight chitosan, purchased from Sigma-Aldrich (448877-250G, Batch 07918TE) was dissolved at 8% (w/v) in 100% trifluoroacetic acid (TFA) (Fisher, O4901-500) by stirring for 15 hours at 45C. Methylene chloride (MeCl) (Fisher, D143-1) was added drop wise into the chitosan solution, while stirring, to the final (v/v) ratio of TFA: MeCl, 80:20. The viscosity of the chitosan electrospinning solution was measured using Rheometric Scientific (T.A. Instruments) Stress Rheometer SR 200 25mm PPS parallel plate at room temperature (25C - 30°C). The viscosity measurements were performed at various time points after initial mixing of the chitosan in the TFA (2, 15, 24 hours and 7 days).

2.2.2 Chitosan Nanofibers Fabrication and Diameter Characterization

The electrospinning apparatus used to generate the chitosan nanofibers included a syringe pump to pump the chitosan solution through an 18 gauge, 1 inch long metal needle at 3-4ml/hour. A high voltage power supply of 25-30kV was attached to the needle and a grounded aluminum collector plate was positioned 25-30cm from the tip of the needle. The chitosan solution was placed in the syringe and electrospun at room temperature (25C to 30°C) and relative humidity of (20-30%). The chitosan nanofibers were placed under vacuum for 24 hours to remove the remaining solvent from the nanofibers. The fiber diameter distribution was determined using scanning electron microscopy (SEM) using a LEO 1530 Gemini microscope. The chitosan nanofibers were carbon sputter-coated and examined by the SEM. Diameters of 195 fibers, 65 fibers from three

electrospun samples were measured. Sigma Scan Pro software was used to analyze the average fiber diameter.

2.2.3 Mechanical Tensile Testing

The Young's modulus and ultimate tensile strength were determined using an Instron uniaxial tensile testing equipment model 3343. The chitosan nanofiber matrices were prepared into rectangular strips (60x20mm). The relative humidity was 20-30%, gauge was set to 20mm and cross head speed of 10mm/min was used. All the strips were tested until complete rupture with a 100N load cell at room temperature (25-30°C).

2.2.4 Fiber Swelling Assay

The chitosan nanofiber mats were prepared into squares (20x20x0.15 mm3) and neutralized in a basic solution composed of 15N ammonium hydroxide and 100% ethanol (1:1 v/v) for 30 minutes. The nanofibers were then washed with deionized water three times, each time for 10 minutes. The nanofibers were placed in phosphate buffer solution, PBS; pH 7.2 and incubated at 37°C and 10% CO_2. The PBS solution was changed every 3 days. At certain time points (days 1, 7, 14, 21, 28) the nanofibers' diameter distribution was analyzed by SEM. The fiber diameters were quantified using Nikon Imaging Solutions (NIS)-elements basic research software (v.3-448). Three chitosan sample duplicates was used for each time point and a total of ~190 measurements were used to analyze the diameters.

2.2.5 In Vitro Lysozyme Degradation Assay

The chitosan nanofiber matrices were prepared into squares (20x20x0.15 mm3) and neutralized as mentioned above. The degradation of the chitosan nanofibers was assessed

by incubating them in egg-white lysozyme (MP Biomedicals LLC, CAT#100834) dissolved at 4mg/ml in PBS, pH 7.2, at 37°C and 10% CO_2. At specific time intervals (days 7, 14, 21, 28) the matrices were removed from the lysozyme solution, washed with water, vacuum dried for 24 hours, and weighed. The degradation profile was illustrated using the weight loss percentage of the dried sample before and after degradation.

2.2.6 Fourier Transform Infrared Spectroscopy

Fourier transform infrared (FTIR) analysis was done using the Perkin Elmer FTIR-ATR 100 series. The spectra were analyzed in the 400-2000cm-1 range with a resolution of $4cm^{-1}$ and 30 scan repeats. Unprocessed chitosan powder, film cast from the electrospinning solution and electrospun nanofibers were analyzed. The chitosan films were cast by pouring 2ml of the chitosan electrospinning solution in an uncoated p35 Petri dish and allowed to air dry in the chemical hood for over 48 hours.

2.2.7 Thermal Analysis via DSC and TGA

Thermogravimetric analysis (TGA, TA instruments model Q50, New Castle, DE) was performed in an inert atmosphere (dry nitrogen, flow rate 40ml/min), 10°C/min heating rate and maximum temperature of 300°C. Differential scanning calorimetry (DSC, TA instruments Q100, New Castle, DE) was performed in sequential double scans on each sample. The first scan was to remove the water in the sample which was followed immediately by the second scan.

2.2.8 Molecular Organization Analysis via XRD

Chitosan powder, cast film and electrospun nanofibers were analyzed by X-ray diffraction (XRD) using an X'pert Pro Diffractometer (PW3050/60, Philips, Netherlands).

Monochromatized Cu K (1.54056A) X-ray source was used to irradiate the samples with a step size (2-theta) of 0.05°, scan step time of 1.0 sec and 2-theta range of 0-60°. The operating voltage and current were 45kV and 40mA, respectively.

2.3 Results

2.3.1 Fiber Fabrication and Diameter

At 2hrs after mixing 8% (w/v) chitosan in 100% TFA, the viscosity of the solution was 12,700cP (Figure 2.2). The addition of the organic solvent MeCl to the solution caused the viscosity to dramatically drop to 1,400cP. It was observed that the viscosity of the electrospinning solution decreased as time progressed. Attempts at electrospinning the solution at 2hrs failed because the viscosity was too high for the solution to be smoothly pumped out of the needle.

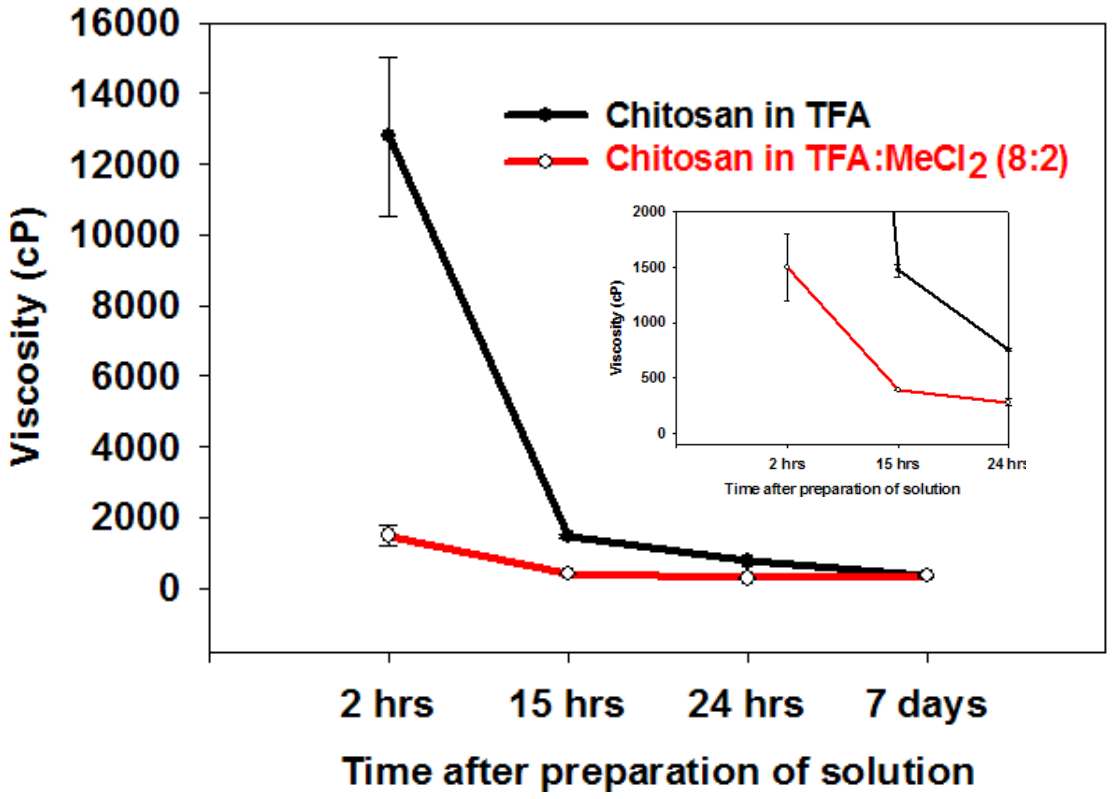

Figure 2.2 The viscosity of chitosan solutions using two solvents, (black: TFA, red: TFA and Methylene Chloride) post initial mixing. Graph insert is a close-up of the 2-24hrs.

The optimized viscosity of the electrospinning solution that enabled the generation of smooth bead free fibers from chitosan was around 300 cP; this was achieved after 12-15 hours of stirring. Beyond this stirring window, the solution is not

viscous enough and electrospinning attempts led to the formation of droplets onto the metal collector. The optimized chitosan fiber matrices had an average fiber diameter of 188±59nm and mat thickness ~150-200µm (Figure 2.3).

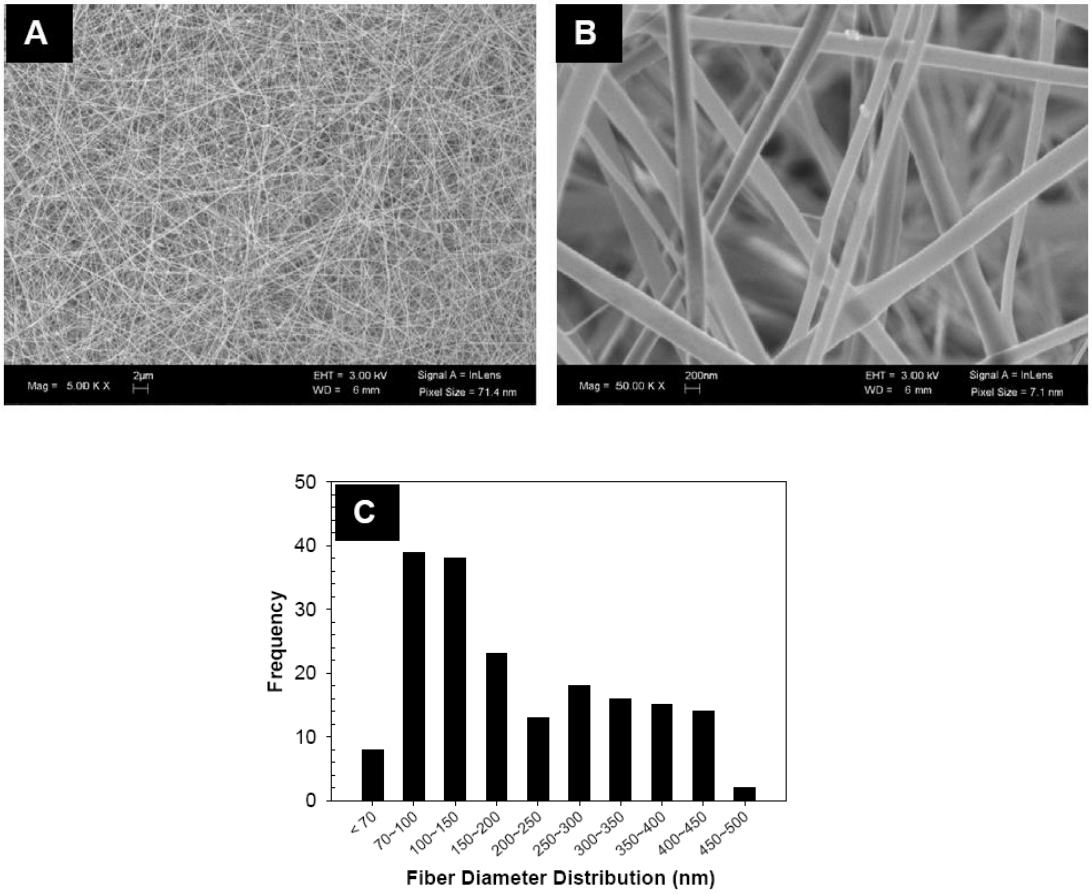

Figure 2.3 SEM images of vacuum dried electrospun pure chitosan prepared from 8% (w/v) chitosan dissolved in trifluoroacetic acid/methylene chloride (8:2) solution. (A) 5000 X original magnification (B) 50,000X original magnification. (C) Fiber diameter distribution of the chitosan nanofibers. Average diameter and standard deviation was 188± 59nm.

2.3.2 Instron Tensile Testing

The uniaxial tensile properties of the chitosan nanofiber matrices were examined using an Instron. The stress-strain profile, seen in Figure 2.4, of the matrices resulted in an evolving stress-strain modulus. During the initial phase of the tensile loading, the elastic

modulus was 20.4MPa ± 5. Following further tensile loading onto the matrices, the stress-strain modulus increased significantly to 62.3MPa ± 5. The matrices ruptured at an ultimate tensile strength of 2.20 ± 0.37.

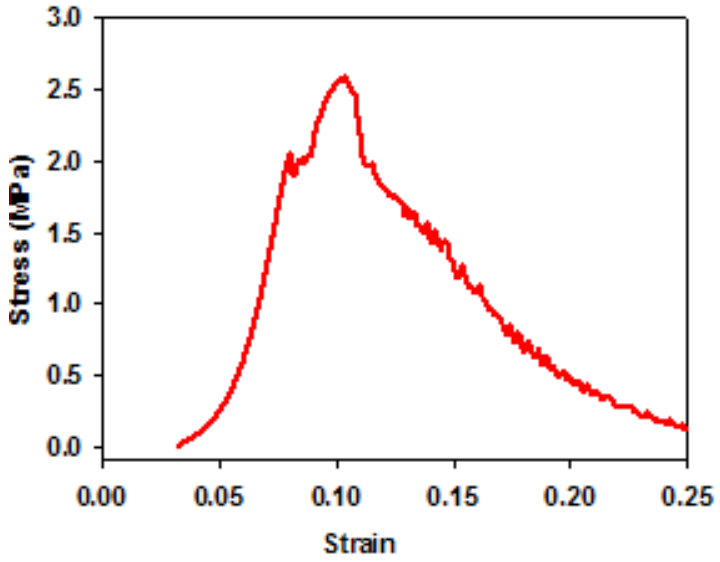

Figure 2.4 The stress-strain profile of electrospun pure chitosan nanofibers under uni-axial tensile stress applied using an INSTRON apparatus at 25°C.

2.3.3 Fiber Morphological Stability

The structural stability of the fibers was monitored during PBS incubation over 28 days. The freshly formed fibers (0 day incubation) displayed an average diameter of 188±59nm. Table 2,1, demonstrates that the increase in fiber average diameter and the diameter distribution range.

Table 2.1 Average Fiber Diameters of the Pure Electrospun Chitosan Nanofibers Incubated in Phosphate Buffered Solution at 37°C and 10% CO_2

PBS incubation days	Fiber diameter (average ± std dev)
0	188nm±59
1	258nm±106
7	356nm±213
14	442nm±172
21	446nm±213
28	405nm±143

The widening of the diameter distribution range suggests the presence of a range of swelling properties within the electrospun chitosan fibers. Hence, some fibers swell faster than others, as seen in Figure 2.5 which shows the distribution electrospun chitosan fiber diameters at several time intervals up to 28 days of PBS incubation.

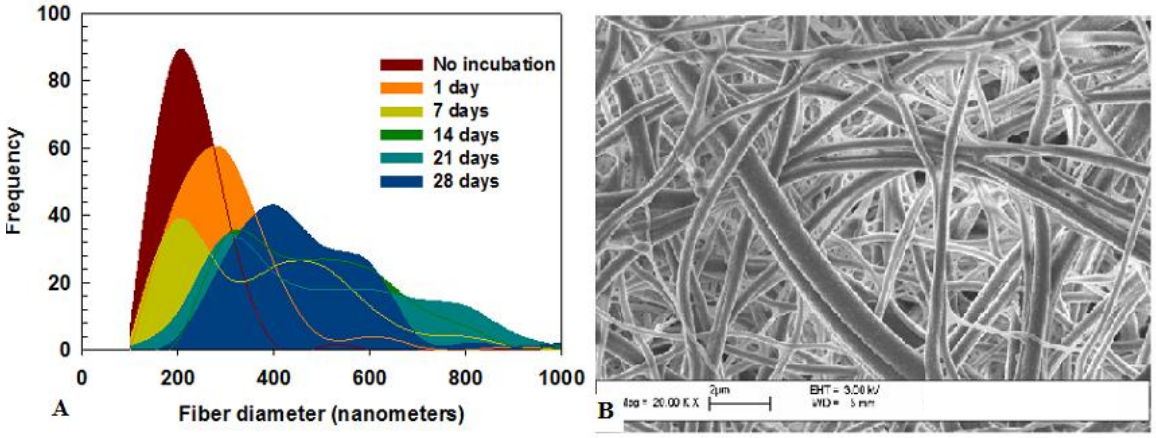

Figure 2.5 (A) Graphical representation of the widening of the electrospun chitosan fiber diameter distribution during 0, 1, 7, 14, 21, 28 days of PBS incubation. (B) SEM of electrospun chitosan fiber after 28 days of PBS incubation showing the increased fiber diameter distribution, 20, 000X original magnification. (50 measurements were performed from 3 replicate samples for each time period).

2.3.4 Fiber In Vitro Degradation Assay

The degradation study demonstrated significant changes in the rate of degradation with time. The chitosan fiber matrices showed the highest rate of degradation during the first 7 days by displaying 30% dry weight loss. The matrices lost a further 13% dry weight during the following 21 days. The degradation profile shown using percent weight loss in Figure 2.5A demonstrates that the degradation rate is initially rapid followed by a slow degradation phase. The SEM micrographs (Figure 2.6B) of the chitosan matrices treated with lysozyme for 28 days depict that some of the fibers have maintained their smooth cylindrical morphology while others have degraded into textured, beaded film structures.

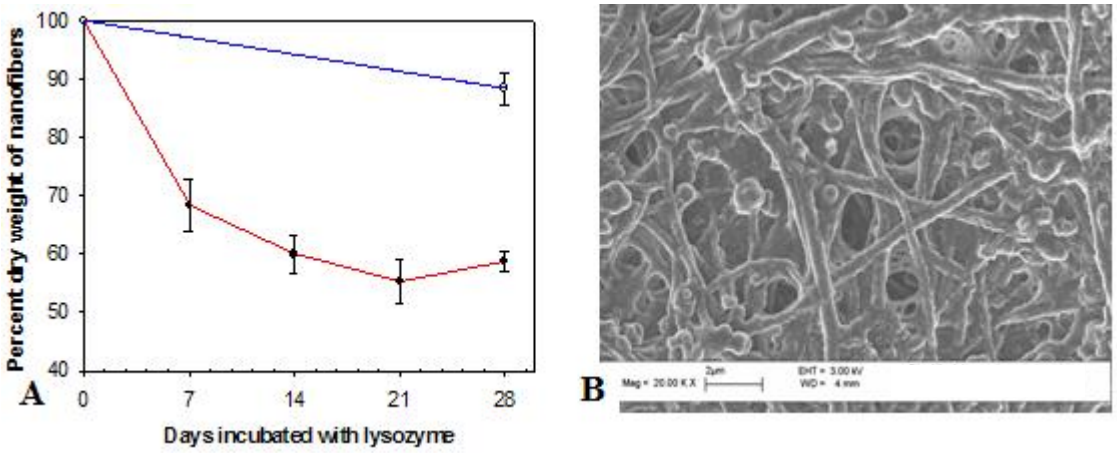

Figure 2.6 (A) Graphical representation of dry weight loss percentage of electrospun chitosan nanofibers during in vitro bio-degradation assay using lysozyme. (Blue: no lysozyme, red: with lysozyme) (B) SEM of the electrospun chitosan nanofibers after 28 days incubation in lysozyme solution, 20,000X original magnification.

2.3.5 Fourier Transform Infrared Spectroscopy

The FTIR spectra of the chitosan film and electrospun fibers show the presence of CH and CH_2 peaks at 719-793 cm^{-1} and NH amine peak at 834cm^{-1} which are absent from the unprocessed chitosan powder spectra (Figure 2.7). The NH amide band was shifted downward from 1560-1553 cm^{-1} in the powder to 1525-1515cm^{-1} in the electrospun fibers, similarly the CO amide band shifted from 1673-1668cm^{-1} to 1648-1640cm^{-1}.

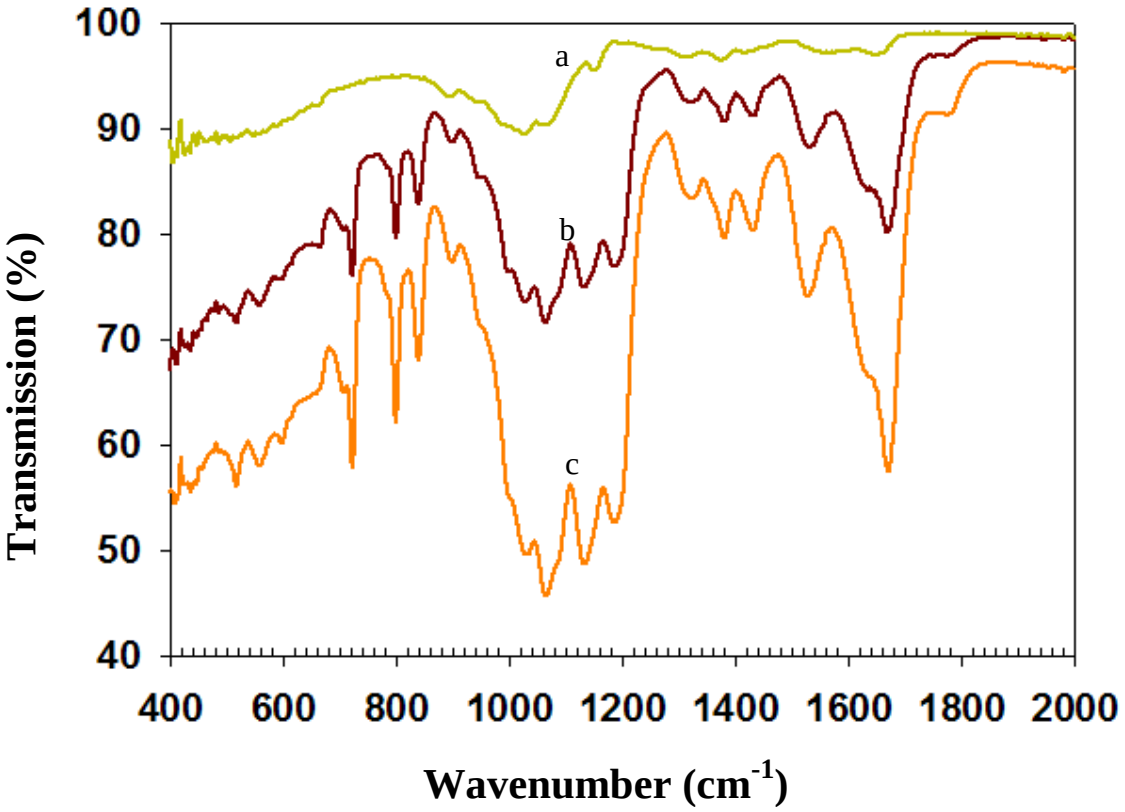

Figure 2.7 FT-IR analysis of the unprocessed (a) chitosan polymer powder, (b) cast film from the electrospinning chitosan solution, and the (c) electrospun chitosan nanofibers.

2.3.6 Thermal Analysis

Changes in heat flow in the sample and degradation temperatures were studied using DSC and TGA. The unprocessed chitosan powder and the electrospun chitosan fibers were compared. DSC profiles demonstrated broad endothermic events with peak maxima at 90°C for the electrospun chitosan fibers and 140°C for the chitosan powder during the first scan. The second DSC scan illustrated a change in heat flow at 120°C, and a broad endothermic event at 230°C followed by another event at 250°C. The chitosan powder's second DSC profile demonstrated a change in heat capacity at 200°C and an endothermic event at 270°C (Figure 2.8A).

TGA showed an initial weight loss that plateaus in both the electrospun chitosan fibers and powder. Further weight loss of the electrospun chitosan fibers started at a temperature of ~150°C as compared to the powder which started at ~280°C (Figure 2.7B).

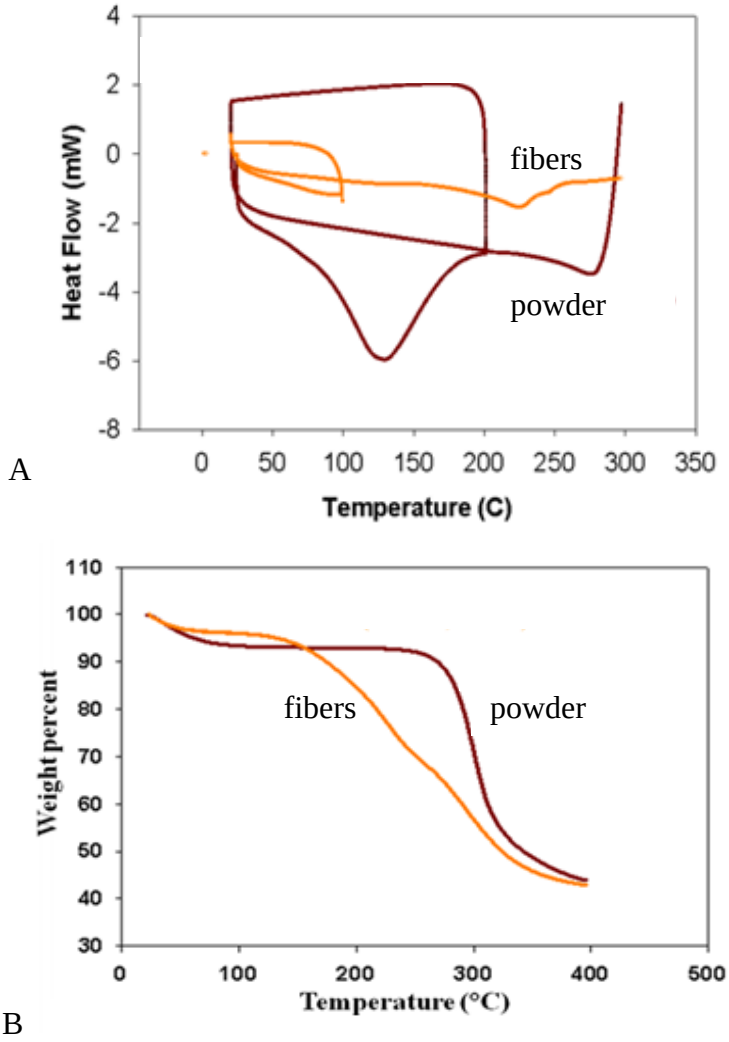

Figure 2.8 (A) Differential Scanning Calorimetric analysis and (B) Thermal Gravitational Analysis of the unprocessed chitosan powder and the electrospun chitosan nanofibers.

2.3.7 X-ray Diffraction

As depicted in Figure 2.9, the unprocessed chitosan powder had two broad peaks at 2-theta = 10.2° and 19.9°, in addition to a broad background halo. The cast film from the

chitosan electrospinning solution resulted in one broad peak at 2-theta= 19.9°. The electrospun chitosan fiber XRD pattern resulted in the lowest intensity peak at 2-theta = 19.9, two very sharp and intense peaks at 2-theta = 38.3° and 44.5° and the lowest amount of background halo.

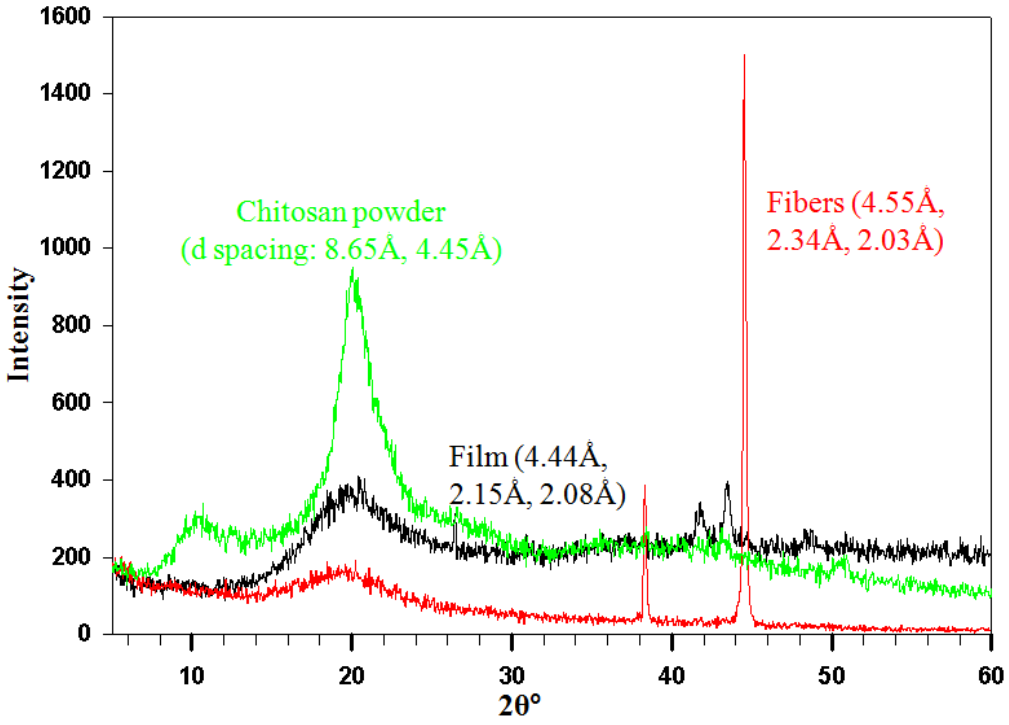

Figure 2.9 X-ray diffraction patterns of unprocessed chitosan powder, chitosan film and electrospun chitosan nanofibers.

2.4 Discussion

The goal of this section of the research was the fabrication and characterization of the physical, chemical, and thermal properties of electrospun chitosan.

Electrospinning is a complex process affected by many parameters including the nature of the solvent's volatility and polarity, polymer concentration and molecular weight, surface tension, pump flow rate, voltage applied, electrospinning distance,

temperature, and humidity. The viscosity of the electrospinning solution is vital in forming bead-free continuous fibers because very low viscosities imply that the solution is materially deficient to produce a continuous fiber. Solutions with very high viscosities would clog the metal needle and prevent the continuous flow of the polymer solution. The polymer solution's viscosity is influenced by the intermolecular interactions between the polymeric chains. Chitosan's high viscosity is caused by the strong and numerous 3-dimensional networks of hydrogen bonds between the amine and hydroxyl groups [74, 75]. TFA is used to dissolve chitosan because it forms amine salts with chitosan's C2-amine groups [76]. The addition of the organic solvent methylene chloride causes a significant drop in the viscosity. This can be attributed to the disruption of the hydrogen bond network allowing the mobilization of the polymer chains under the influence of the electrical field.

The reduced viscosity allows the chitosan solution to flow continuously out of the capillary tip enabling the formation of continuous bead free fibers. The continuous drop in viscosity of the chitosan-TFA solution is attributed to the acid hydrolysis of the chitosan which is accompanied by the solution changing color from yellow to dark brown. This is due to the release of free glucoasmines which causes browning of the solution [77] . The acid hydrolysis of chitosan decreases the molecular weight, which in turn decreases the density of polymer entanglements present in the solution. These polymer entanglements are necessary for holding the polymer chains together to form a coherent fiber. As a result, with increase polymer degradation, the solution's spinnability decreases preventing the formation of a continuous fiber. Hence in electrospinning of chitosan form

an acidic solvent there exists a time period (12 to 15 hours in our study) prior and beyond which chitosan could not be electrospun.

The random orientation of the electrospun chitosan nanofibers leads to the deposition of fiber entanglements within the matrix. These entanglements get engaged when the fiber matrix experiences tensile stress giving rise to a characteristic stress-strain modulus behavior. In Figure 2.4, the Young's modulus of the chitosan nanofibrous matrix increased as the stress applied increased. The increase in the modulus can be explained by the increase in the number of fiber entanglements engaged as more and more fibers are being pulled on. Ultimately, the chitosan nanofibers rupture causing the entanglements to fail.

Due to chitosan's high hydrophilicity and likelihood to form hydrogels, the structural integrity of the chitosan nanofibers was investigated in PBS for 28 days. Hydrophilicity is a vital feature of chitosan's appeal as a biomaterial as it enhances the production of the extracellular matrix and enhances homeostasis of wounds by accelerating blood clotting [78]. The incubation of the chitosan nanofibers in PBS resulted in swelling of some of the fibers while maintaining the cylindrical fibrous morphology. Some fibers swelled at a rapid rate, while others swelled at a slower pace or not at all. The variety in swelling behavior of the chitosan nanofibers can be explained by the differences between the chitosan inter-molecular hydrogen bonds. The fibers that exhibit inter-sheet hydrogen bonding prevent the chitosan from swelling and retaining water. While the fibers in which the inter-sheet hydrogen bonding is absent will swell and retain water [31].

Chitosan can be degraded by a variety of enzymes in vitro such as chitinase, chitosanase, lysozyme, collagenase and pectinase [79-81]. In vivo, lysozyme attacks chitosan's acetylated residues and hydrolyze its glycosidic bonds. Lysozyme is released from phagocytic cells such as macrophages and neutrophils [82]. The degradation by-product of chitosan are aminosugars which are non-toxic, non-immunogenic, and completely absorbed by the body through glycosaminoglycans and glycoprotein metabolic pathways or excreted [83]. Figure 2.6 A show that the fibers undergo an initial phase of rapid degration followed by a phase of slower degradation. SEM micrographs shown in Figure 2.6 B, depict that some fibers have completely lost their cylindrical morphology and transformed into a film like structure, while others have maintained their fibrous structure. The bi-phasic degradation model of the electrospun chitosan can be explained using the fiber swelling, XRD, and FTIR data. Correlating the degradation and swelling test results, it can be suggested that the fibers that exhibit rapid swelling also exhibit faster degradation rates.

FTIR spectra of the electrospun chitosan nanofibers show bond vibration peaks of the amine and alkane groups that were absent in the unprocessed chitosan powder. This suggests that the 3-dimensional hydrogen bond network that immobilized these groups in the chitosan powder was disrupted during electrospinning. In addition, the electrospun chitosan's amide bands have shifted to higher frequencies compared to the chitosan powder indicating that the polymer chains have changed their physical organization compared to the powder [84].

DSC results showed that the electrospun chitosan nanofibers have a change in heat flow at a lower temperature compared to the unprocessed chitosan powder. This

implies that the chitosan polymer chains in the unprocessed powder are physically organized in a different manner compared to the electrospun chitosan nanofibers. The thermal degradation behavior of chitosan is complex as it consists of dehydration, deacetyaltion and chain scission. The unprocessed chitosan powder started thermal degradation at a higher temperature compared to the electrospun chitosan fibers. This can be attributed to the fact that the electrospun chitosan fibers which were prepared from the TFA containing solution have undergone some degradation. During the electrospinning process, the acid hydrolysis of the chitosan chains and the remaining acidic solvent within the fibers will catalyze the degradation of the chitosan nanofibers as compared to the chitosan powder, as seen in Figure 2.8.

The XRD data, Figure 2.9, supports the FTIR data as it indicates a more ordered molecular organization in the electrospun nanofibers as compared to the unprocessed chitosan powder. There are six polymorphs that have been proposed for chitosan: tendon, annealed, 1-2, L-2, form I and form II [85].The two peaks with lattice angles of 10.2° and 19.9° are attributed to the equatorial (100) and (020) reflections seen in the ‘L-2’ chitosan polymorph [86]. The L-2 organization of chitosan chains is significantly disrupted in the electrospun chitosan nanofibers because of the high speed elongational flow and rapid vitrification that occurred during electrospinning. Electrospinning altered the molecular arrangement of the chitosan polymer chains and organized them with two uniform d-spacings. However, some of the L-2 morphology still remains within the electrospun samples. This diversity in molecular organization within the chitosan nanofibers might contribute to the bi-phasic degradation profile and varying fiber swelling rates.

2.5 Conclusion

Pure electrospun chitosan nanofibers were fabricated and analytically characterized. The electrospinning of pure chitosan fibers was successfully reproduced by optimizing the stirring time of the chitosan in the TFA solution, which is correlated to the viscosity of the solution. The characterization results suggest that electrospinning of chitosan alters its molecular organization in a manner that produces two main types of polymer confirmations One type of polymer confirmation allows fiber swelling and rapid degradation by lysozyme. However, the other polymer confirmation swells and degrades at a much slower rate. Based on these observations, electrospinning of chitosan affects its behavior as a scaffolding biomaterial in vitro.

CHAPTER 3

CHITOSAN BIOLOGICAL PERFORMANCE AND VASCUALRIZATION

3.1 Introduction

Many cellular processes, including the differentiation, proliferation, and survival, of adhesion dependent cells are affected by their attachment to the extracellular matrix. The adhesion and interaction of cells to their surrounding is mediated by a variety of transmembrane receptors, integrin being one of the most heavily studied and understood adhesion receptor. Integrins not only attach the cells to the extracellular matrix but they also act as a signal relay center where extracellular mechanical cues are internalized via interaction with cytoskeleton actin microfilaments and intermediate filaments [87]. However, these transmembrane integrin adhesion links also serve as a signaling pathway cluster where focal adhesion enters activate various signaling molecules including FAK, Src, and paxillin [88].

Unique amino acid sequences, for example arginine-glycine-aspartic acid (RGD), present in the extracellular matrix mosaic of proteins provide the binding site for integrins. Hence, the integrin-mediated adhesion of cells onto biomaterials is dependent on the ability of the extracellular matrix proteins to adsorb and adequately present these amino acid binding sites to the cells. The biomaterial surface characteristics that affect protein adsorption include hydrophilicity/hydrophobicity, chemistry, surface charge and charge density, texture, crystallinity, and rigidity [89-92]. There are numerous techniques to improve the cytocompatibility of biomaterial surfaces including adsorption,

blending and crosslinking of proteins; however the main objective of those techniques is to present extracellular matrix motifs to the cells to enhance integrin binding.

One of the most interesting biomaterial induced cell processes is the tubulogenesis of endothelial cells on Matrigel. This biomaterial induced phenomenon is the result of culturing endothelial cells on a gel material that consists of harvested rat chondrosarcoma extracellular matrix [93]. Matrigel contains many extracellular matrix proteins such as laminin-1, collagen IV and peptides C16 and A13 which are known to be proangiogenic signals [94]. However, it is unlikely that Matrigel will ever reach the patient's bedside since it is very costly and tumor derived.

As a matter of fact, a major challenge in the engineering of any tissue, especially myocardial tissue, is the incapability of providing sufficient blood supply immediately post implantation. Engineering grafts for thick complex tissues such as cardiac tissue require adequate vasculature to sustain physiological requirements since the diffusion limit for oxygen is 100-200 μm [95]. This challenge is intensified when engineering a physiological demanding tissue such as the myocardium. The native myocardial tissue is supplied by rich vasculature which is necessary to quench the immense demand for oxygen and nutrients required for its continuous vigorous contractile activity.

In addition to serving as conduits for blood supply, endothelial cells are vital for promoting cardiomyocyte survival and function [96]. Neureglin secreted by endothelial cells affect cardiomyocyte survival, proliferation and hypertrophic growth through the phosphatidylinositol-3-kinase-AKt pathway [97-99]. Furthermore, cardiac endothelial cells influence cardiomyocyte contractility by the secretion of numerous modulators, such as nitric oxide which affects cardiomyocyte inotropism [100], endothelin causes

cardiomyocyte constriction [101] and platelet derived growth factor (PDGF) affect cardiomyocyte development [102].

Several approaches have been investigated to vascularize cardiac grafts. Capsi et al. seeded human Embryonic Stem Cell derived endothelial cells (hESC-EC) or Human Umbilical Vein EC (HUVEC) on PLLA/PLGA porous scaffolds along with embryonic fibroblasts and were able to depict some vascularization [97]. Radisic et al. covalently immobilized angiogenic factors VEGF and angiopoietin-1 onto collagen sponges resulting in an increase in infiltration of murine embryonic heart endothelium cells into the scaffold and an elongated cellular morphology [103]. Okano et al. were able to show in growth of vasculature from HUVEC sheets into fibroblast sheets that were stacked on top of each other [104]. Dvir et al. were successful in showing that maturing their cardiac Matrigel incorporated constructs on a blood rich membrane, rat omentum, enabled the formation of functional blood vessel networks [105]. Matrigel is a biological mixture of the basement membrane extracted from rat chondrosarcoma ECM, which makes it unfavorable for patient use [93]. While these vascularization attempts have led to limited success, the goal of engineering a favorable technique to generate 3-D vasculature networks within scaffolds remains elusive.

This section of the research focused on the improvement of chitosan's cytocompatibility by adsorbing fibronectin on its surfaces. In addition, a novel technique of inducing tubulogenesis in endothelial cells was developed by using fibronectin and chitosan's hydrogel-like nanofibers' characteristics. This is a very important and translatable part of the research as the vascularization of biomaterial scaffolds can be used as a platform technology for vascularization of many regenerative constructs.

3.2 Methods

3.2.1 Fibronectin Adsorption on Chitosan Films and Nanofiber

In order to evaluate fibronectin adsorption on chitosan, 24-well tissue culture dishes were coated with 1% chitosan and dried for 1 hr before neutralization with 0.2 M ammonium hydroxide. Fibronectin (Sigma) solutions of different concentration (0 μg/ml, 0.6 μg/ml, 1.2 μg/ml, 5 μg/ml, 10 μg/ml, and 20 μg/ml in deionized water) were added into the dishes and incubated for 1 hour. The chitosan nanofibers were treated with fibronectin solution (10 μg/ml) for 1 hour at 37C and 10% CO_2 incubator. The relative amount of adsorbed fibronectin was characterized by fluorescent staining intensity analysis using the primary rabbit anti-fibronectin (Sigma) and the secondary anti-rabbit IgG, alexa fluor 488 (Invitrogen).

3.2.2 Cell Seeding on Chitosan Film and Nanofibers

Primary ventricular cardiomyocytes were isolated from 1-day-old neonatal Wistar rats (Charles River Laboratories, MA) using a collagenase procedure as described previously [106]. Briefly, the pups are anesthetized by spraying with ethanol and incubating in the refrigerator for 10 minutes. The beating heart is excised from a small abdominal incision. The hearts are washed with PBS and minced into small pieces. The minced heart pieces are then treated in 0.12% collagenase II solution in a series of digestion incubations each for 15 minutes and the dissociated cells are collected in 5% Horse serum. The harvested cells are then separated according to Percoll gradient. The cardiomyocyte layer is cultured on 0.1% gelatin coated dishes.

Cardiomyocyte culture medium consists of DMEM (Gibco, Gaithersburgh, MD) with 10% FBS (Biowest, Miami, FL), 2 mM L-glutamine (Gibco), insulin/transferrin/selenious acid (ITS; 5 μg/mL, 5 μg/mL, 5 ng/mL, respectively) (Invitrogen), and 2% penicillin/streptomycin (Gibco). Murine 3T3-J2 fibroblasts (purchased from Howard Green, Harvard Medical School, Boston, MA), were maintained in 60-mm tissue culture dishes in DMEM plus 10% FBS and 2% penicillin and streptomycin. Rat heart microvascular endothelial cells (MVEC; purchased from VEC Technologies, Rensselaer, NY) and rat liver sinusoidal endothelial cells (LSEC; isolated from adult rat liver), were maintained in DMEM supplemented with 10% FBS, 2 mM L-glutamine, ITS, 2% penicillin/streptomycin, and 10 ng/mL vascular endothelial growth factor (VEGF, R & D Systems, Minneapolis, MN). Culture medium was changed every three days.

For the 2-D cell cultures, the chitosan or chitosan/Fibronectin adsorbed films were prepared in 24-well tissue culture dishes, as described in Section 2.2. Cells were seeded at a density of ~25,000 cells/cm^2 on the films in 0.5 mL of culture medium. For 3-D cell cultures, the nanofibers were treated with fibronectin solution (10 μg/ml) for 1 hour to adsorb fibronectin on the fibers. The nanofibers were then soaked in culture medium for about 5 minutes prior to cell seeding. The suspended cells (fibroblasts, cardiomyocytes, or endothelial cells) in culture medium were directly seeded at a density of ~300,000 cells/cm^2 on separate chitosan nanofibrous mats with 300 μl of medium and incubated for about 1 hour before adding further medium to allow for better cell entrapment and attachment. The mats were incubated in a 10% CO_2, 37 ^oC incubator and the medium was changed every 3 days.

3.2.3 Tube Formation on Different Types of Gels

Endothelial cell tube formation was tested on two different gel substrates: collagen gel and Matrigel ™. 0.1% (w/v) gelatin was prepared in deionized water. The gelatin solution was warmed in a 37°C water bath before use. Collagen gel (BD Biosciences) was prepared by mixing 1.2 mg/ml collagen solution with 10X DMEM at 9:1 ratio (v/v) at ice temperature and keeping it on ice until use. The Matrigel solutions (BD Biosciences) were maintained at ice temperature until use.

150µL of each gel type substrate was added into a well of a 24-well plate and the gels were incubated at 37°C and 10% CO_2 for 45 minutes to allow for gelation. The EC cells were cultured in endothelial cell medium, containing DMEM supplemented with 10% Fetal Bovine Serum, 2% Penicillin/Streptomycin, 10g/ml Vascular Endothelial Growth Factor (VEGF) and 1X Insulin-Transferrin-Selenium (ITS). The cells were cultured at 37°C and 10% CO_2 in p60 tissue culture dishes and harvested at 75-90% confluency.

For harvesting cells, the p60 tissue culture dishes were washed twice with 3mL of Phosphate Buffer Solution (PBS) and then incubated with 1mL 1X trypsin (SAFC Biosciences, cat # 59428C-500ml) at 37°C and 10% CO2 incubator for 10 minutes. The cells detached from the surface of the tissue culture dish after the incubation period. With the help of a pipette, the surface of the tissue culture dish was further washed with the trypsin-cell suspension to ensure the detachment of any remaining attached cells. In addition, the trypsin-cell suspension was gently mixed with a pipette to cause the disintegration of any cells that might have detached as clusters. The trypsin was then neutralized by the addition of 5mL of the endothelial cell media and centrifuged at room

temperature for 10 minutes at a speed for 850 revolutions per minute. The supernatant was discarded and the cell pellet was re-suspended in 1mL of endothelial cell media.

The cells were counted using a hemocytometer and seeded on top of the gel substrates at a density of 10,000 cells/cm^2. The total volume of endothelial cell media added to the wells was 250µL. Tube formation was checked using light microscopy every 24 hours of culture. Tube formation was classified as the alignment of the endothelial cells behind each other in a train-like fashion and the physical transformation of the cells into elongated or tubular morphologies. Light phase images were captured using Nikon camera (model number 150365). The media was changed every three days.

3.2.4 Tube Formation on Chitosan Nanofibers

The chitosan nanofibers were prepared into squares (20x20x0.15 mm^3) and neutralized in a basic solution composed of 15N ammounium hydroxide and 100% ethanol (1:1 v/v) for 30 minutes. The nanofibers were then washed with deionized water three times, each time for 10 minutes. The fibers were then incubated for 1 hour in 10µg/ml human fibronectin solution (BD Biosciences). The fibers were washed with endothelial cell media prior to cell seeding. Endothelial cells were seeded at a density of 200,000 cells/cm^2 directly on the fibronectin-coated chitosan nanofibers.

3.2.5 Cell Attachment and Spreading Evaluation

The samples were washed with PBS and fixed with 4% paraformaldehyde for 20 minutes at room temperature. After washing with PBS, the samples were permeabilized in 0.2% Triton X-100 in PBS for 10 minutes. The samples were then washed with PBS and incubated in blocking buffer (PBS/10% FBS/1% BSA) for 30 minutes. The primary antibody was then added and incubated for 60 minutes at room temperature. The samples

were washed with PBS and then incubated with the secondary antibody for 60 minutes. The samples were then washed and examined with fluorescence microscopy (Nikon). The primary antibodies used were mouse anti-vinculin (Millipore, 1:200 dilution), mouse anti-α-sarcomeric actin (Invitrogen, 1:50 dilution), and rabbit anti-connexin 43 (Sigma, 1:1000 dilution). The secondary antibodies used were donkey anti-mouse IgG, alexa fluor 488 and donkey anti-rabbit IgG, alexa fluor 594 (Invitrogen).

For the distribution of actin microfilaments, cells were stained by incubating fixed and permeabilized cultures with 0.1 μg/mL rhodamine phalloidin (Sigma) for 30 min. In some cases, cells were counterstained with 4, 6-diamidino-2-phenylindole (DAPI; Invitrogen) for nuclear staining. In order to verify the adsorption of fibronectin onto chitosan, the samples were stained for 1 hr at room temperature with rabbit anti-fibronectin. After washing twice with PBS, the samples were incubated with alexa fluor 488 conjugated anti-rabbit IgG, and washed twice with PBS. Cell viability on the nanofiber scaffolds was examined by a live/dead viability/cytotoxicity kit (Invitrogen).

3.2.6 Scanning Electron Microscopy (SEM)

The cell seeded nanofibers scaffolds were examined with SEM. The samples were fixed with 2.5% gluteraldehyde for 24 hours at 4 ^{o}C. The samples were then washed with PBS and serially dehydrated with 50%, 70%, and 100% ethanol for 15 minutes each. This was done to allow gradual dehydration of the cells preventing loss of cellular structural integrity. The samples were then vacuum-dried for about 6 hours. The samples were coated with carbon and observed with SEM.

3.2.7 Live/Dead Cell Staining

Calcein AM/Ehidium homodimer live/dead cell stain was used to visualize the cells on the 2-D gel substrates and 3-D chitosan nanofibers. To stain the cells, the cell culture media was changed and Calcein AM and Ehtidium homodimer (Invitrogen L3224) were added at 1µL/ml of media to the cultures. The cultures were then placed at 37°C and 10% CO_2 for 10 minutes prior to capturing images using the fluorescent microscope. Nuclear DAPI stain was also used to stain the nuclei of the cells by adding 1µL /ml of culture and incubated for 10 minutes.

3.2.8 Safranin-O Staining

Safaranin-O was used to stain the sulfated glucosaminoglycans present in the chitosan mats. The cell seeded mats were treated with 4% paraformaldehyde (Electron Microscopy Sciences, 15715-S) for 20 minutes. 2mL of the Safranin-O dye was then added to the culture dishes and incubated at room temperature for 10 minutes. The chitosan mats were then washed with water at least three times. Light images were then captured using the Nikon light microscope.

3.3 Results

3.3.1 Fibronectin Adsorption on the Chitosan Scaffolds

It is known that cellular attachment to biomaterials is enhanced by immobilizing fibronectin by adsorption. To establish the concentration at which chitosan is saturated by fibronectin adsorption, immunofluorescent staining of adsorbed fibronectin using varying concentrations (0 μg/ml to 20 μg/ml) was performed. Figure 3.1 illustrates an increase in observed fluorescence intensity with fibronectin concentration, which suggests that fibronectin adsorption on chitosan coated wells is dependent on the concentration of the fibronectin solution. There was a steady increase in the amount of adsorbed fibronectin as the concentration increases and the adsorption plateaus beyond 10 μg/ml. As a result, the 10 μg/ml solution was used to adsorb fibronectin on the chitosan nanofibers for improved cell adhesion.

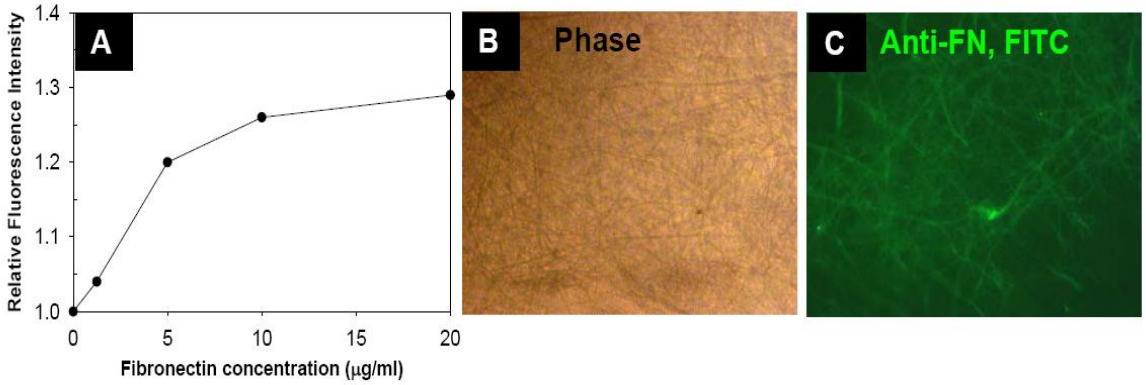

Figure 3.1 Fibronectin adsorption on chitosan. (A) Relative fluorescence intensity of adsorbed fibronectin on chitosan coated tissue culture dishes at various fibronectin concentrations by immunofluorescence staining. (B and C) Light phase and immunofluorescence staining for anti-fibronectin of chitosan nanofibers adsorbed by fibronectin solution (10μg/ml) at 200X original magnification.

3.3.2 Effect of Fibronectin on Cellular Morphology and Cytoskeletal Organization

In order to investigate the effect of fibronectin immobilization on chitosan material in cell cultures, the morphology and cytoskeletal protein distribution of endothelial cells and cardiomyocytes were monitored on 2-D chitosan films with and without fibronectin adsorption. The optical microscopy and fluorescent staining in Figure 3.2A (endothelial cells) and 3.2C (cardiomyocytes) indicates that the cells maintain a rounded morphology, minimal vinculin (focal adhesion) expression, and a diffused F-actin cytoskeletal organization when cultured on chitosan film. In contrast, the cells cultured on fibronectin coated chitosan films demonstrated enhanced cellular spreading, significant increase in vinculin expression and a well organized fibrous F-actin cytoskeleton (Figures 3.2B and 3.2D).

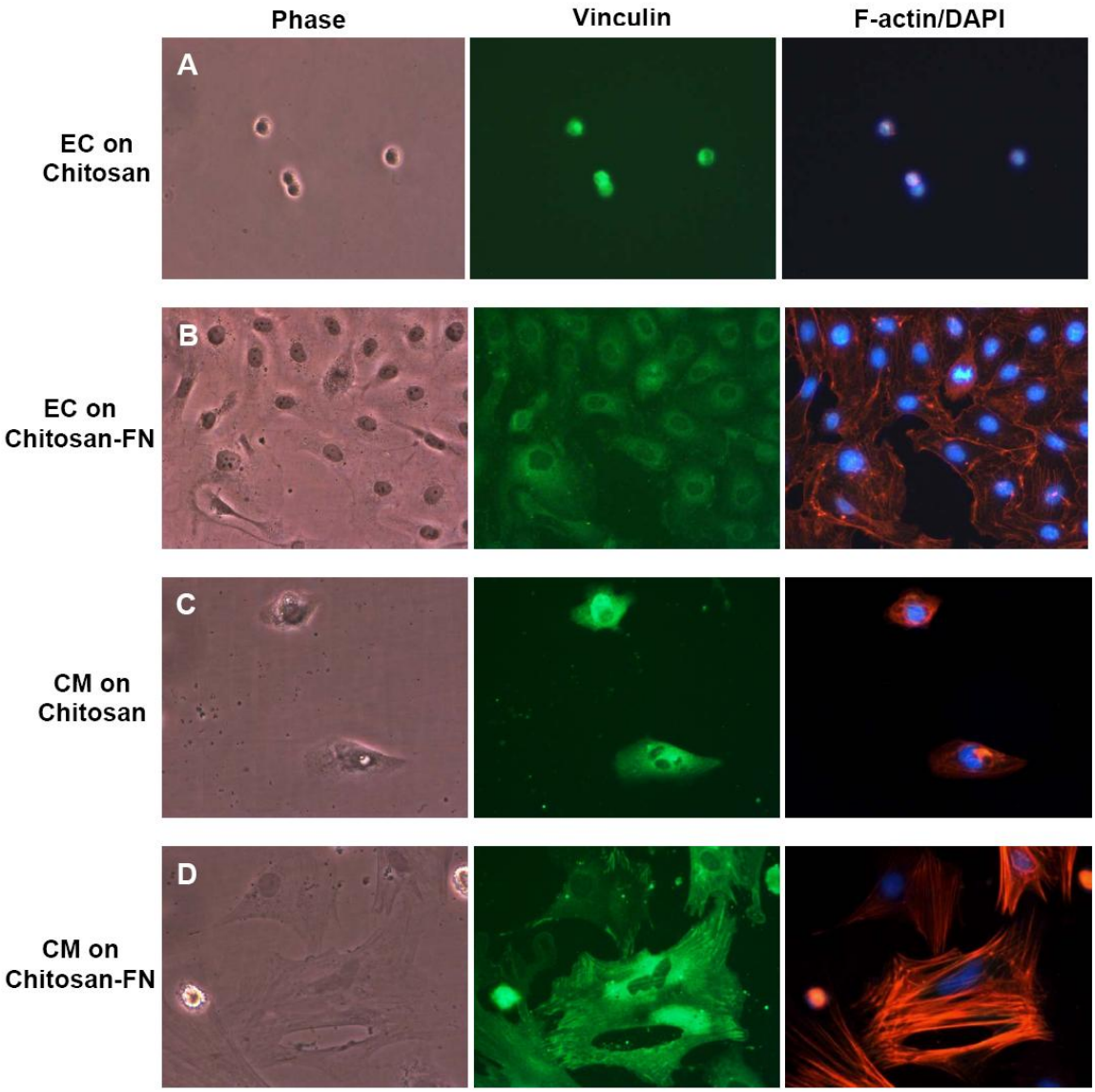

Figure 3.2 Morphology, Vinculin (focal adhesion) expression, and cytoskeletal F-actin organization of (A and B) endothelial cells (EC) and (C and D) cardiomyocytes cultured on chitosan and chitosan-fibronectin coated tissue cultured dishes (day 2 cultures). Light phase contrast and immunoflourescence staining images for Vinculin (green), cytoskeletal F-actin (red), and nuclear DAPI (blue) of endothelial cells and cardiomyocytes . 200X original magnification.

Similarly, the endothelial cells seeded on non-coated chitosan nanofibers retained their circular morphology and did not attach to the nanofibers. Figure 3.3 depicts SEM micrographs of the endothelial cells seeded on coated and non-coated chitosan nanofibers.

It is clear that the cells extend pseudo pods and attach onto the nanofibers when they are coated with fibronectin.

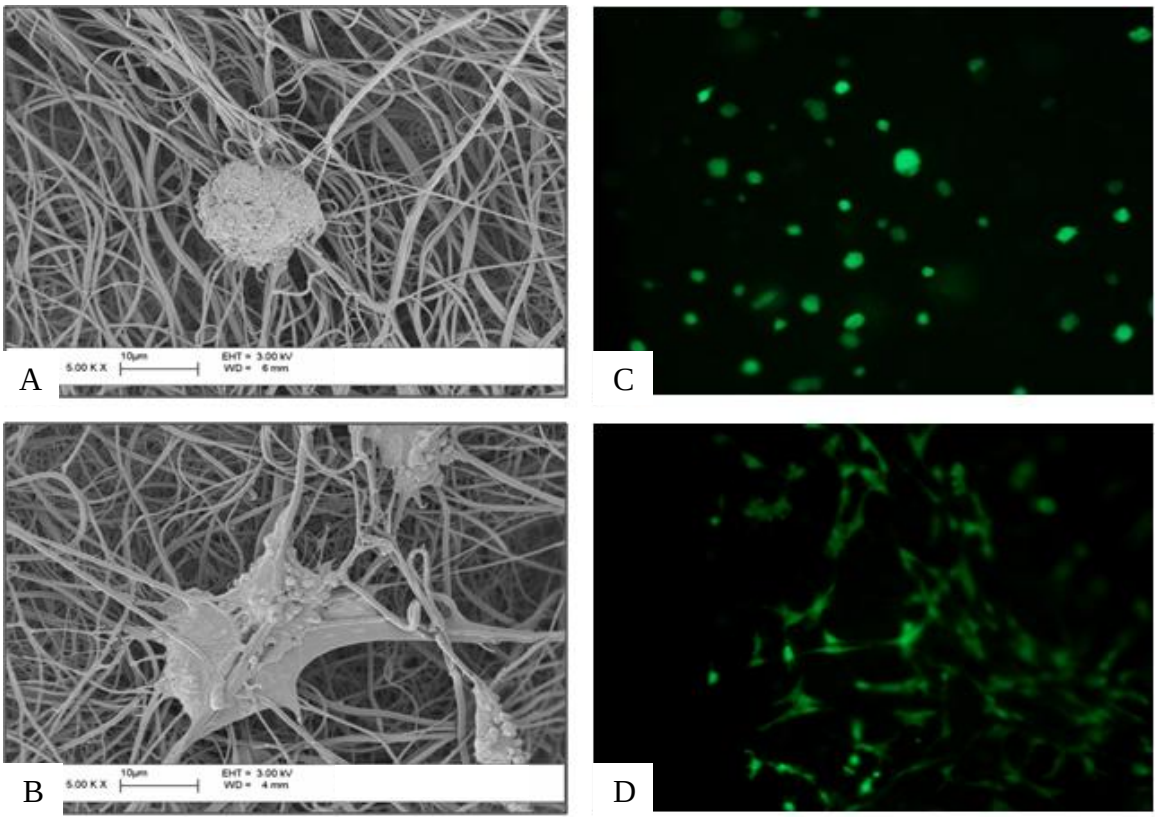

Figure 3.3 (A and B) SEM micrographs of non-coated and fibronectin coated chitosan nanofibers seeded with endothelial cells (MVEC) after 1 day culture. 5,000X original magnification. (C and D) Live cell calcein AM stained endothelial cells cultured on non-coated and fibronectin coated chitosan nanofibers after 1 day culture. 200X original magnification.

3.3.3 Characterization of Cellular Behavior in Chitosan Nanofibrous Mats

Assessment of cellular viability and morphology was performed to evaluate the cytocompatibility of electrospun chitosan nanofibrous mats and their potential as cellular scaffolds. Three day culture of fibroblasts on the chitosan nanofibers demonstrated endothelial cells, and cardiomyocytes were seeded onto fibronectin coated chitosan mats and cultured over three weeks. Figures 3.4A-C depict the live-dead staining of fibroblasts

cultured on the chitosan nanofiber scaffolds, indicating the chitosan nanofibers do not adversely affect cell viability. Some cells formed filopodia-like extensions to attach to the fibers, assisting them in spreading inside the chitosan nanofibrous scaffold, Figure 3.5 A. In addition, the SEM images exhibit the formation of a film-like material surrounding the densely seeded areas, indicating the secretion and immobilization of cell secreted ECM components.

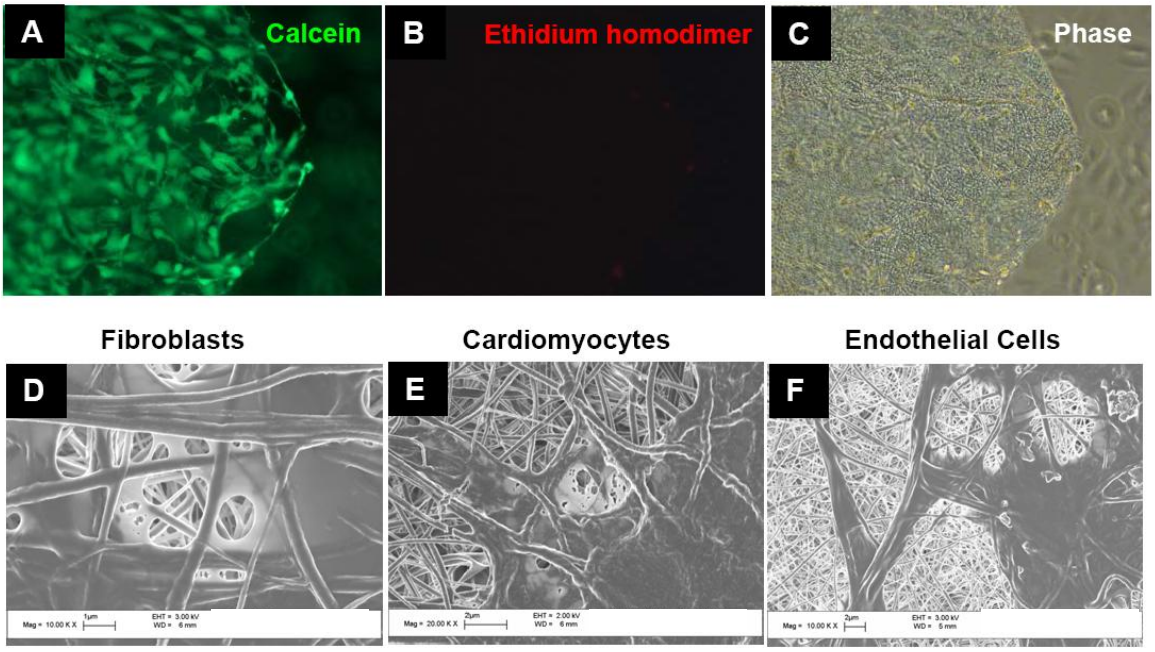

Figure 3.4 (A) Live cell calcein AM staining (B) Dead cell Ethidium homodimer staining and (C) Light phase image of 3T3-J2 fibroblasts cultured on chitosan-fibronectin adsorbed nanfoibers for 4 days. 200X original magnification. (D-F) SEM images of fibroblasts, cardiomyocytes, and endothelial cells cultured on chitosan-fibronectin adsorbed nanofibers after three weeks of culture.

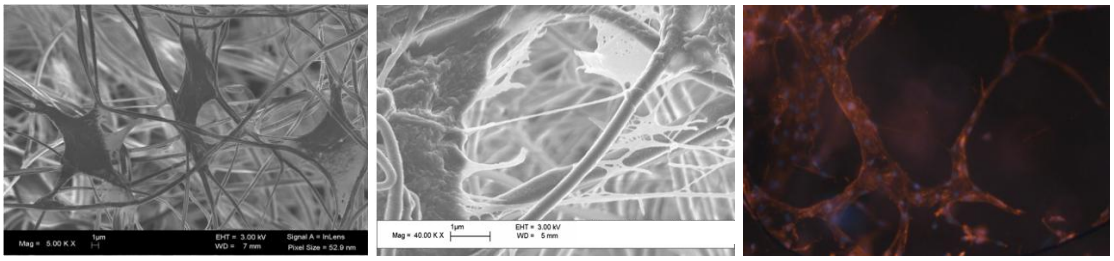

A B C

Figure 3.5 (A) SEM micrograph of fibroblasts cells after 9 day culture in chitosan nanofibers showing the extension of pseudopods to attach to physically attach to the fibers, 5000X original magnification. (B) SEM micrograph of fibrous extracellular matrix extruding from the cell surface to the chitosan nanofibers, 40 000X original magnification. (C) Immunofluorescent staining of cytoskeletal f-actin (red) and nuclear DAPI (blue) to illustrate fibroblasts day 9 cellular distribution within the nanofibers, 100X original magnification.

3.3.4 Effect of Gel Type and Cell Density on Tube Formation from Endothelial Cells.

Endothelial cells (LSEC) cultured on Collagen gel did not results in any tube formation at either cell densities as seen in Figure 3.6. However, when LSEC were cultured on Matrigel, the low density culture (50,000 cells/cm^2) resulted in disconnected tubes as opposed to the high density system which resulted in an interconnected tubular network.

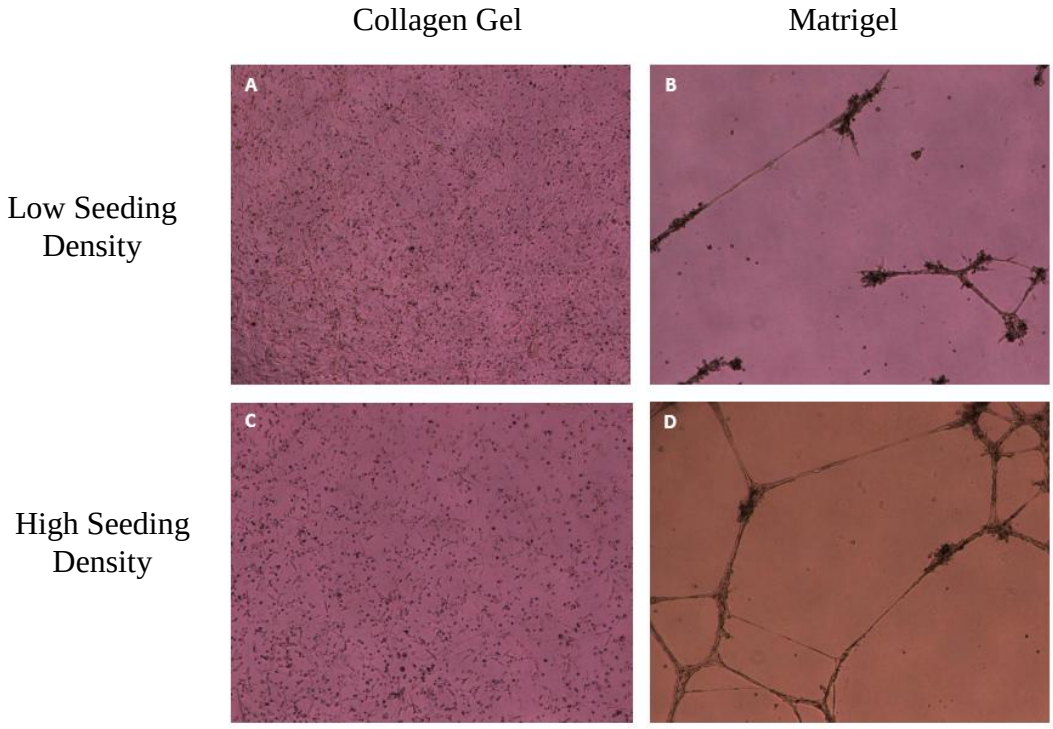

Figure 3.6 Light phase images of LSEC cultured on collagen gel and Matrigel at low and high cell densities. (A) collagen at 50 k cells/cm^2 (B) Matrigel at 50 k cells/cm^2 (C) collagen at 125 k cells/cm^2 (D) Matrigel at 125 k cells/cm^2. All images were captured after 24 hours of incubation at 37°C and 10% CO_2. 40X original magnification.

LSEC cultured on chitosan nanofibers were observed to form interconnected networks over three weeks of culture periods. Capillary-like network formations increased over time and they remained structurally stable and viable up to 21 days as seen in Figures 3.7 A-D.

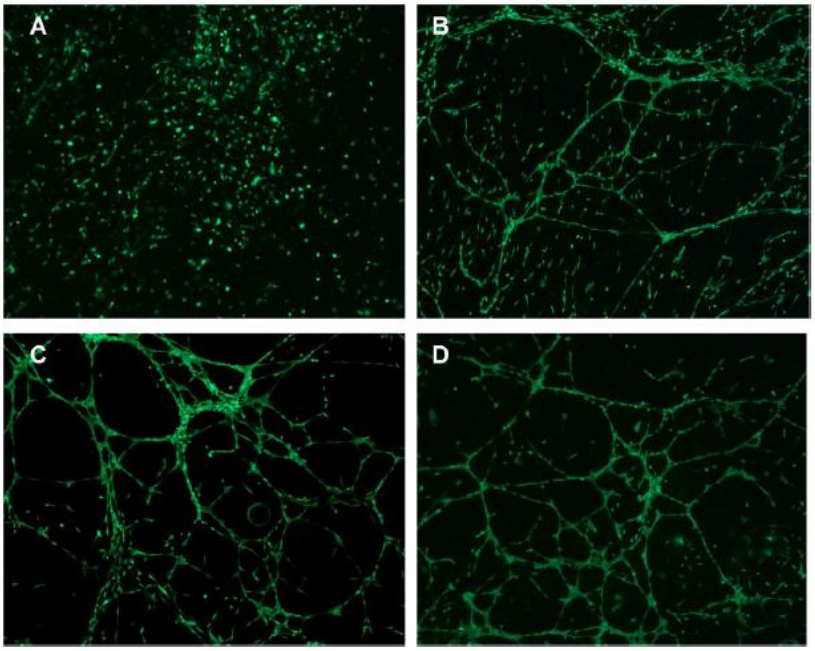

Figure 3.7 Calcein AM live cell staining of LSEC cultures in chitosan nanofiber mats (A) day 1 (B) day 7 (C) day 14 and (D) day 21. 40X original magnification.

It is evident from Figures 3.7 and 3.8 that the endothelial cells seeded on the fibronectin coated chitosan nanofibers were able to migrate and develop intercellular alignment that enabled the cells to attain connected tubular morphologies.

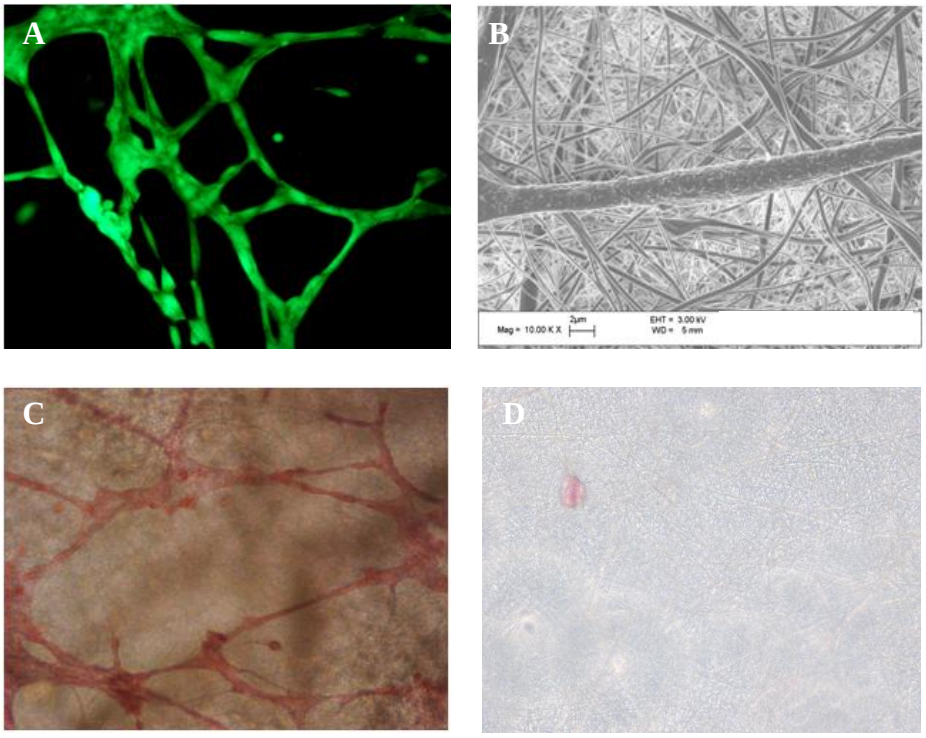

Figure 3.8 LSEC tube-like network structures in the chitosan nanofibers 80 k cells/cm^2 on day 14 (A) Calcein AM live cell stained image, 200X (B) Scanning electron micrograph, 10,000X and (C) Safranin-O stained image of cell seeded scaffold (D) Safranin-O stained image of scaffold without cells (control), 200X.

3.4 Discussion

The goal of this section of the research was to improve the cytocompatibility of chitosan using fibronectin adsorption and induce tubulogenesis of endothelial cells.

Fibronectin adsorption on chitosan improved cellular attachment significantly. This was possible because of chitosan's cationic nature which does not cause the loss of the biological activity of the adsorbed fibronectin. Proteins not do denature when adsorbed on hydrophilic surfaces such as cationic chitosan as their confirmation is not altered significantly [107]. Hence the fibronectin was adsorbed on the chitosan films which significantly improved cell attachment and spreading. The improved cellular

attachment was successfully accomplished on the chitosan nanofibers as well. It is clear that the fibronectin adsorbed chitosan nanofibers induce the cells to form pseudopods and attach to the nanofibers. Furthermore, the cells seeded on the nanofibers began to migrate through the inter-fiber voids, secrete their own extra cellular matrix and form a coherent 3-dimensional tissue-like network. This migration of cells through the scaffold was clearly demonstrated using tubulogenesis which is the intercellular alignment of cells to form interconnected tubes.

Vascular morphogenesis, among other complex cellular processes, is orchestrated via interaction between the cell's genetic information and the interstitial extracellular matrix (ECM). The ECM functions as a dynamic scaffold providing malleable biological and physical cues that coordinate the cells' fate. In this study, first we investigated the effect of two different gel substrates and cell seeding densities on one of the stages of vascular morphogenesis: intercellular alignment into tubes. In addition, 3-dimensional tube formation was studied on fibronectin adsorbed chitosan nanofibers.

Collagen gel and Matrigel were the two gel substrates investigated. Gelatin is derived from denatured natural collagen. Collagen is the fibrous structural protein component of the natural in vivo ECM. Matrigel is the reconstituted soluble basement membrane extract derived from the Engelbreth-Holm-Swarm (EHS) sarcoma. This laminin-rich basement membrane gelatinous substrate contains other ECM components such as collagen IV, heparin sulfate proteoglycan, entactin/nidogen, and growth factors [108].

As seen in Figure 3.6, LSEC resulted in intercellular alignment only when they were cultured on Matrigel. These results might be caused by differences in the biological

nature of cellular attachment to the gel substrates. Matrigel is rich in laminin which induces endothelial cell alignment and capillary tube formation by interacting with the cell using the YIGSR sequence in the B1 chain and RGD sequence in the A chain [109]. Furthermore, it has been reported that cellular traction on the Matrigel surface generates narrow tracks on the gel surface along which the endothelial cells can migrate to align themselves into tubes [110].

Interconnected tubular formation was evident when the cell seeding density was increased from 50,000 cells/cm^2 to 125,000/cm^2 on 100% Matrigel as evident in Figure 3.6. The endothelial cells' morphogenesis into the vascular phenotype requires the coordination of multiple behaviors including migration, proliferation, intercellular alignment and adhesion and the generation of a lumen [111]. Endothelial cells' behavior, survival and proliferation is heavily dependent on the integrin mediated interactions with basement membrane components within the Matrigel [112].

In addition, tube formation was investigated on the chitosan nanofibers without the use of Matrigel. Figure 3.7 clearly demonstrates that LSECs have migrated across the nanofibers and have aligned themselves linearly to form interconnected network tubes. The intercellular alignment of LSEC on the nanofibers could be the result of physical cues from the architecture of the nanofibers. As the endothelial cells attach and migrate across the chitosan nanofibers they can cause traction by pulling on the nanofibers and communicate mechanically with neighboring cells about their spatial organization. The cells can sense the mechanical signals through their transmembrane ECM receptors such as focal contact sites [113]. The phosphorylation of integrin by protein kinases at these focal contact sites can induce cytoskeletal reorganization which might mediate tubular

morphogenesis [114]. Hence, mechanochemical cues caused by the cells traction on the nanofibers trigger morphogenic signaling that mediates tube formation.

Nevertheless, the influence on the morphogenesis of endothelial cells by the substrate's architecture is one of the factors amongst an elusive matrix of factors that synchronize vascular morphogenesis. To our knowledge this is the first report of endothelial tube formation on 3-dimensional chitosan nanofibers without the use of the most commonly used angiogenic gel substrates such as Laminin and Matrigel.

3.5 Conclusion

The biological performance of the chitosan nanofibers was successfully improved via fibronectin adsorption. The migration of endothelial cells and intercellular alignment into tubes in the chitosan nanofibers exhibits the immense potential of using chitosan nanofibers as vascularized tissue engineered constructs or in vitro tissue models. In the next section, the vascularized chitosan nanofibers will be impregnated with a cardiomyocyte-fibroblast co-culture system to recreate the myocardial vascularized cellular niche.

CHAPTER 4

VASCULARIZED CARDIOMYOCYTE/FIBROBLAST CO-CULUTRE MODEL

4.1 Introduction

In the adult human myocardium, cardiomyocytes compose about 70% of myocardial tissue volume but only 30% of the cell population [115]. The remaining cell population is mainly composed of fibroblasts, followed by endothelial cells, smooth muscle cells, pericytes, macrophages, and nerve cells [116-118]. The mentioned cell species are organized in a very unique 3-dimensional architecture that optimizes mechanical and electrical coupling enabling the myocardial tissue to sustain its contractile function. The extracellular matrix (ECM) provides a scaffold in which all the cells are spatially coordinated, as seen in Figure 4.1.

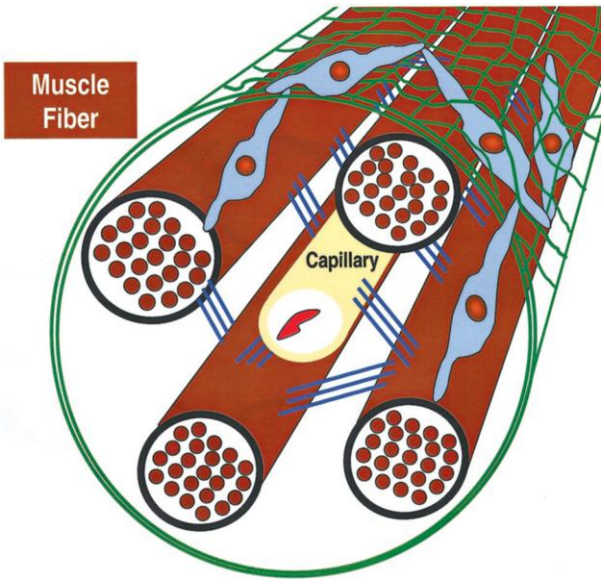

Figure 4.1 Graphical representation of the cardiomyocyte tubules in the native myocardium [119].

Some of the principal challenges of generating a thick functional myocardial construct are maintaining *in vitro* cardiomyocyte function and structure, recreating the

intricate physical and chemical myocardial milieu, and vascularizing the dense construct. In the past section, we were successful in vascularizing the chitosan scaffold with endothelial cells. Hence, in this section, our aim is to impregnate the vascularized chitosan scaffold with cardiomyocytes and fibroblasts to get closer to the in vitro recreation of the cardiac cellular mosaic that can function as a myocardial tissue model. Each cell in this cardiac mosaic performs vital functions that enable the optimum functionality of the cardiomyocytes. For instance, as seen in Figure 4.2, each cell within the myocardium is involved in the secretion of certain extracellular components dependant on the mechanical and neurohormonal cues received by them.

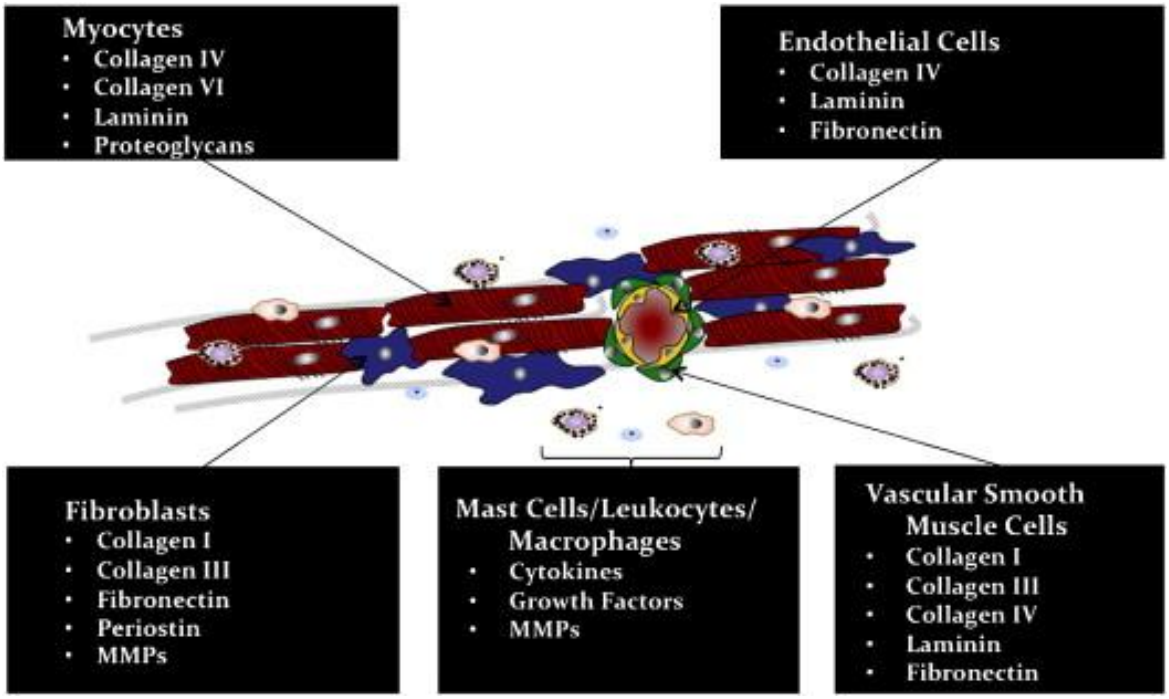

Figure 4.2 Graphical representation of the diverse cellular milieu of the myocardium. The cells have unique and overlapping contributions to the myocardium extracellular constituents [120].

The cardiac fibroblasts produce the heart's interstitial ECM fibrillar proteins which are predominantly Type I and III collagens and elastin [121]. The fibrous collagen network maintains the structural integrity of the heart tissue as the cardiomyocytes

shorten and the entire tissue contracts [122]. Fibroblasts have also been shown to assist in electrical propagation of the wavefront [123]. Each cardiomyocyte is surrounded by multiple fibroblasts, this close relation is vital for the mechanical and biochemical communication between the two cell types. For instance, the secretion of stretch-induced growth factors from cardiomyocytes activate fibroblasts cell proliferation and collagen synthesis to counteract stress increases [124].

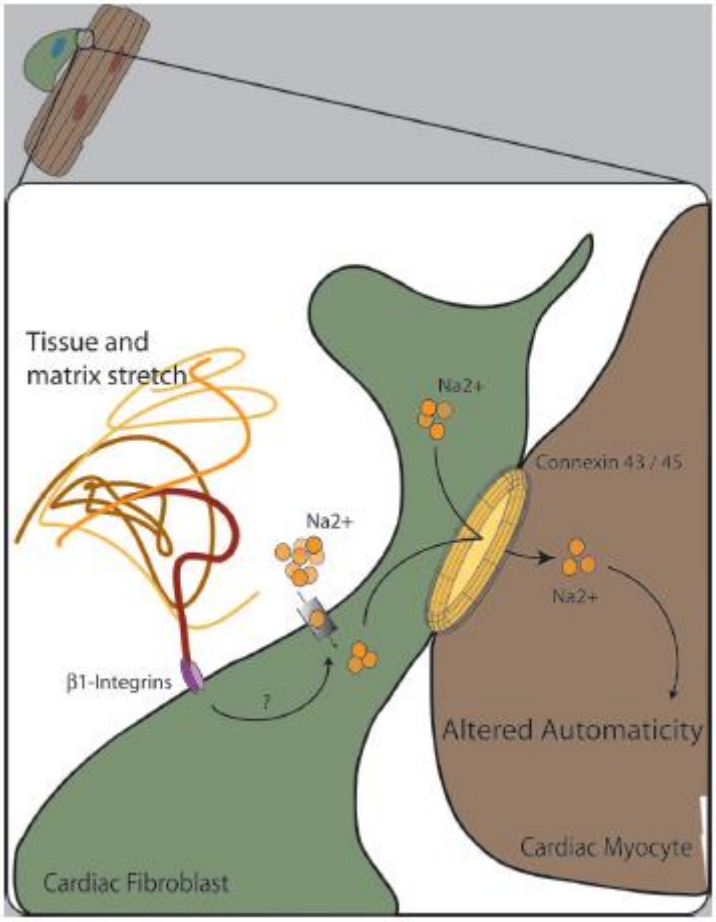

Figure 4.3 Diagrammatic representation of the connexin 43/45 gap junctions between fibroblasts and cardiomyocytes that regulate the syncytial network within the myocardium [125].

Cardiomyocytes form distinct layers that wrap around the contour of the heart. Each cardiomyocyte is about 10-15um in diameter, 100um in length, and are connected

end-to-end in both the longitudinal and transverse directions [117]. The maturation, survival and function of cardiomyocytes are dependent on various physiological cues including the physical and mechanical ECM cues which are relayed through the collagen-integrin-cytoskeletal relation [117]. Endothelial cells populate the complex vasculature networks that perfuse the myocardial tissue. However, endothelial cells functions are not confined to forming the capillary beds but they also affect cardiomyocyte survival, contraction rhythmicity and cardiomyocyte organization via paracrine signaling.

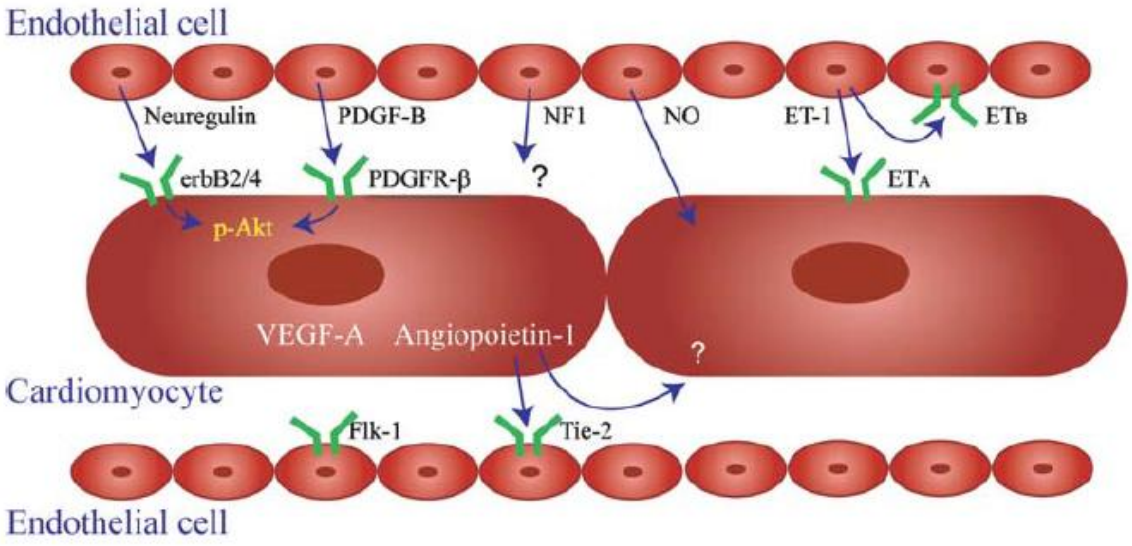

Figure 4.4 Graphical representation of the paracrine and autocrine signaling that constitute endothelial-cardiomyocyte interactions [96].

Simulating the *in vivo* myocardial cellular architecture with fibroblasts and endothelial cells will present the cardiomyocytes with a physiological milieu that is closer to the native environment and hence assist in retaining their function [126, 127]. The intercellular interactions via gap junctions, cell-cell adhesion proteins and paracrine signaling will aid in recreating the *in vivo* cellular communication that is vital in maintaining optimum cardiomyocyte function and survival [128-130]. The 3-D nanofibers will provide a physical matrix with interconnected spaces similar to the

collagenous fibers in the native extracellular matrix. The pre-vascularization of the construct will serve as an *in vitro* perfusion system to supply essential nutrients and oxygen to the core of the scaffold. In addition, the 3-D vasculature will enable endothelial-cardiomyocyte intercellular communication that affect electrical synchronization and contraction rhythmicity [126]. The pre-vascularization of the construct might also help host vasculature to integrate faster into the construct as the construct is already vascularized.

The main objective of this part of the research is to use the fibronectin functionalized and vascularized chitosan nanofibers to create a tri-culture cardiomyocyte-fibroblast-endothelial in vitro cardiac tissue model.

4.2 Methods

4.2.1 Cardiomyocyte Mono- and Co-cultures on Chitosan Films and Nanofibers

For the co-culture studies (cardiomyocytes-fibroblasts or cardiomyocytes-endothelial cells co-culture) in 2-D and 3-D culture systems, cells were seeded at the ratio of 1 to 1, giving a total initial cell number (cardiomyocytes+fibroblasts or cardiomyocytes+endothelial cells) of ~50,000 cells/cm^2 for 2-D and ~600,000 cells/cm^2 for 3-D cultures. (For detailed methodology in terms of chitosan film and nanofiber handling and cell seeding please refer to section 3.2)

4.2.2 Vascularized Cardiomyocyte-Fibroblasts Co-culture on Chitosan Nanofibers:

The chitosan nanofibers were neutralized, sterilized and incubation in fibronectin as mentioned in Section 2.4. LSEC cells were seeded on the chitosan nanofibers at a density of 125,000 cells/cm^2 and cultured for 7 days to allow for tube formation. Cardiomyocytes

and fibroblasts were seeded at a density of 125,000 cells/cm^2 each and cultured for an additional 7 days.

4.2.3 Immunohistochemsitry of Sarcomeric Actin and Connexin-43:

The samples were washed with PBS and fixed with 4% paraformaldehyde for 20 minutes at room temperature. After washing with PBS, the samples were permeabilized in 0.2% Triton X-100 in PBS for 10 minutes. The samples were then washed with PBS and incubated in blocking buffer (PBS/10% FBS/1% BSA) for 30 minutes. The primary antibody was then added and incubated for 60 minutes at room temperature. The samples were washed with PBS and then incubated with the secondary antibody for 60 minutes. The samples were then washed and examined with fluorescence microscopy (Nikon). The primary antibodies used were mouse anti-vinculin (Millipore, 1:200 dilution), mouse anti-α-sarcomeric actin (Invitrogen, 1:50 dilution), and rabbit anti-connexin 43 (Sigma, 1:1000 dilution). The secondary antibodies used were donkey anti-mouse IgG, alexa fluor 488 and donkey anti-rabbit IgG, alexa fluor 594 (Invitrogen).

4.2.4 Calcium Transient Ion Staining:

Calcium indicator, fluo-4 AM (Invitrogen, F-14201) was reconstituted in sterile DMSO to make a stock concentration of 2mM. Using cardiomyocyte media, the stock was diluted to a final working concentration of 4µM. The cells were incubated in the 4µM indicator media for 45 minutes at 37 ^{o}C. The cells were then washed with only cardiomyocyte medium twice before incubating in cardiomyocyte medium for another 30 minutes at 37C. The indicator dye was excited using a 488nm laser. Videos of the Calcium ion staining were captured using Nikon NIS-Elements Basic research_advanced. Pseudocolor images of the Calcium ion fluorescence intensity were captured every

150ms. The intensity of the calcium ion flux was determined by taking the average intensity from 12 pixel image points from each frame and plotting the average intensity over time.

4.3 Results

4.3.1 Co-culture Effect on Cardiomyocytes' Morphology and Gap Junctions

Cardiomyocyte morphology and gap junction formation were monitored via sarcomeric alpha-actin (SA-actin) and connexin-43 (Cx43) staining, respectively. Cardiomyocytes' SA-actin and Cx43 expression was examined on both fibronectin adsorbed chitosan films (2-D) and fibronectin adsorbed chitosan nanofibers (3-D). In each condition, cardiomyocytes were cultured in monocultures (cardiomyocytes only) and co-cultures (cardiomyocytes-fibroblasts or cardiomyocytes-endothelial cells).

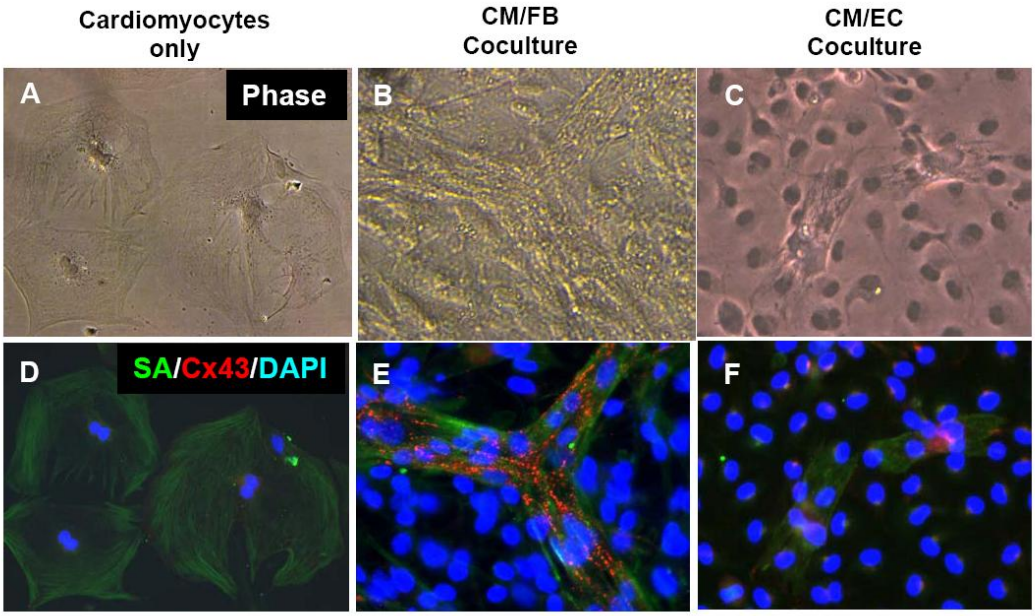

Figure 4.5 Morpholoy and phenotypic characteristics of primary neonatal cardiomyocytes cultured on 2-dimensional Chitosan-fibronectin films. (A,D) Cardiomyocyte monoculture, (B, E) Cardiomyocytes co-culture with fibroblasts, and (C, F) cardiomyocytes with endothelial cells after 7 days incubation at 37°C and 10% CO_2. Cardiomyocytes were immunostained for α-sarcomeric actin (SA) and connecin-43 (Cx43) gap junction expression. 200X original magnification

In the 2-D systems, the cardiomyocyte monoculture (Figure 4.5 A, D) exhibited low expression of SA-actin and the cardiomyocytes lost their structural polarity and acquired a rounded morphology. Gap junction protein Cx43 expression was minimal in the monoculture system, resulting in isolated islands of contractions. In the fibroblasts co-culture system (Figure 4.5 B, E), the cardiomyocytes maintained a highly polar morphology and the SA-actin was strongly expressed along the axis of morphological polarity. In addition, Cx43 expression was the highest in the fibroblasts co-culture which enabled the cardiomyocytes to contract in a tissue-like synchronized manner. The cardiomyocytes co-cultured with endothelial cells (Figure 4.5 C, F) demonstrated a spherical morphology with lower levels of SA-actin and Cx43 expression than those in the fibroblasts co-culture as well as isolated contractions.

To assess the chitosan nanofibers' potential as a cardiac tissue engineering scaffold, the same cardiomyocyte monoculture and co-culture studies were performed on the 3-D chitosan nanofibers. The cardiomyocyte monoculture (Figure 4.6 A, D) and cardiomyocytes-endothelial cell co-culture (Figure 4.6 C, F) did not have any visible SA-actin or Cx43 expression. The cardiomyocyte-fibroblast co-culture resulted in elongated networks of contracting cardiomyocytes with the highest expression of SA-actin and Cx43 (Figure 4.6 B, E).

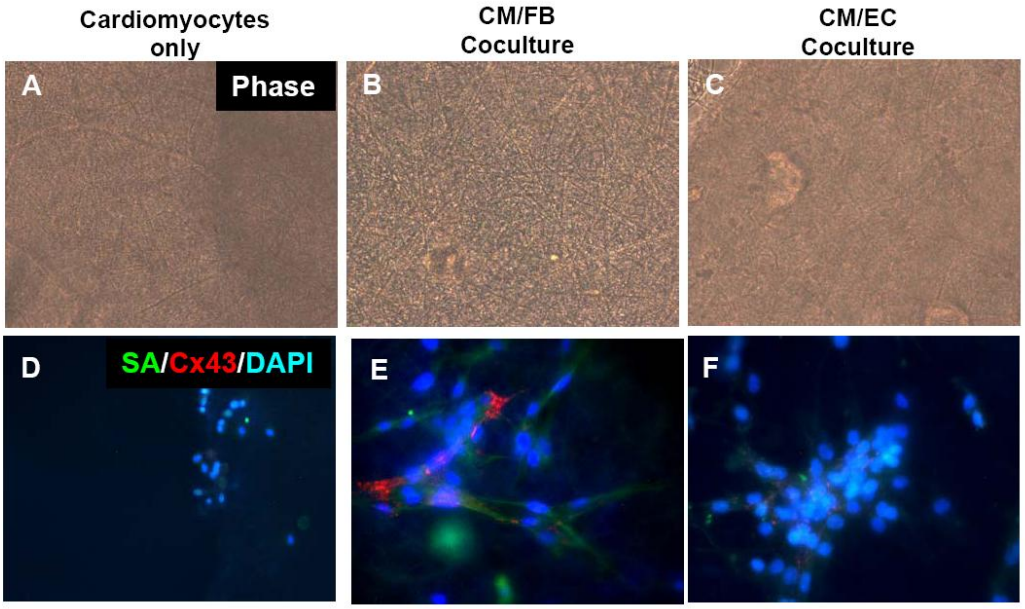

Figure 4.6 Morpholoy and phenotypic characteristics of primary neonatal cardiomyocytes cultured in 3-dimensional chitosan electrospun nanofibrous matrices. (A,D) Cardiomyocyte monoculture, (B, E) Cardiomyocytes co-culture with fibroblasts, and (C, F) cardiomyocytes with endothelial cells after 19 days incubation at 37°C and 10% CO_2. Cardiomyocytes were immunostained for α-sarcomeric actin (SA) and connecin-43 (Cx43) gap junction expression. 200X original magnification

In both 2-D and 3-D cultures on chitosan scaffolds, cardiomyocyte-fibroblasts co-cultures resulted in polarized cardiomyocyte morphology with high levels of SA-actin and Cx43 expression over long-term culture periods. In addition, the fibroblasts co-cultures demonstrated synchronized contractions involving large tissue-like cellular networks, indicating the maintenance of long-term and stable function of cardiomyocytes gap junctions. To our knowledge, the results of the present study provided the first evidence that 3-D chitosan nanofibers can be used as a potential scaffold that can retain cardiomyocyte morphology and function.

4.3.2 Intracellular Calcium Ion Staining

The intracellular calcium ion flux staining was used to assess cardiomyocyte viability and functionality. In the 2-D monoculture system, the cardiomyocyte lose their functionality and morphology within 5-6 days. Figure 4.7 shows the pseudo color time-frame images of the 2-D cardiomyocyte culture system. The image analysis of the calcium flux resulted in a frequency of 8 ± 2 contractions per minute.

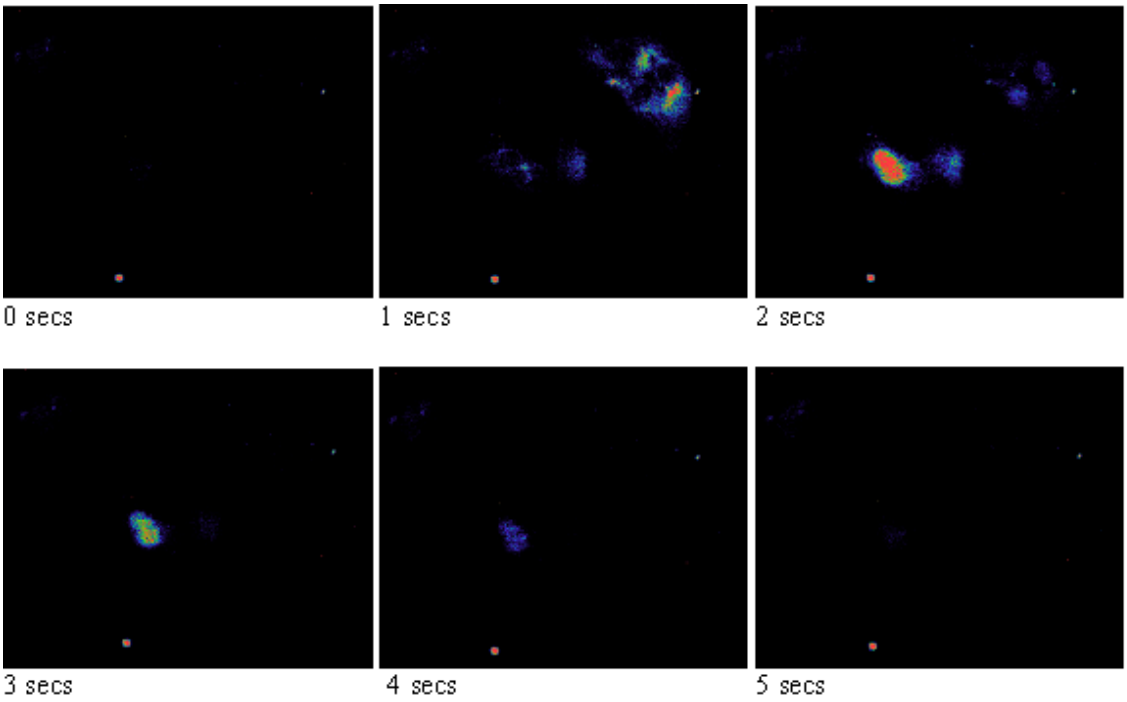

Figure 4.7 Pseudo-color intensity time frame images of intracellular calcium ion flux stained using fluo-4-AM indicator in 2D monoculture of neonatal primary cardiomyocytes cultured for 4 days. 200X original magnification

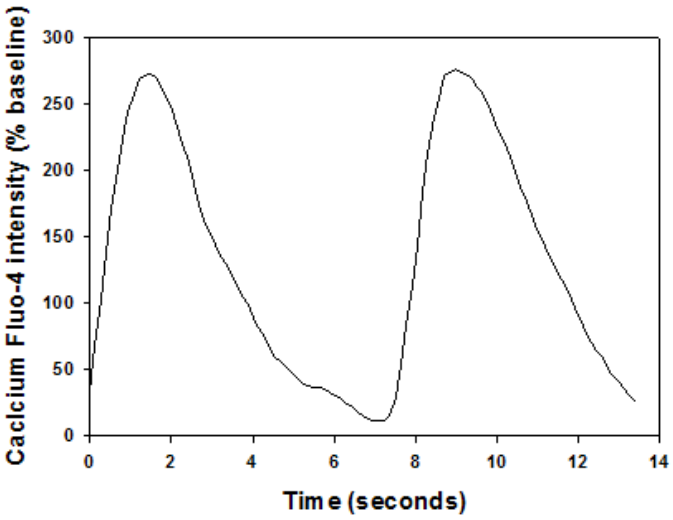

Figure 4.8 Frequency of intracellular calcium ion flux in the 2D monoculture of neonatal primary cardiomyocytes after 4 days in culture.

Figure 4.9 shows the pseudo color time-frame images of the 2-D cardiomyocyte-fibroblast co-culture system. The image analysis of the calcium flux resulted in a frequency of 30 ± 4 contractions per minute.

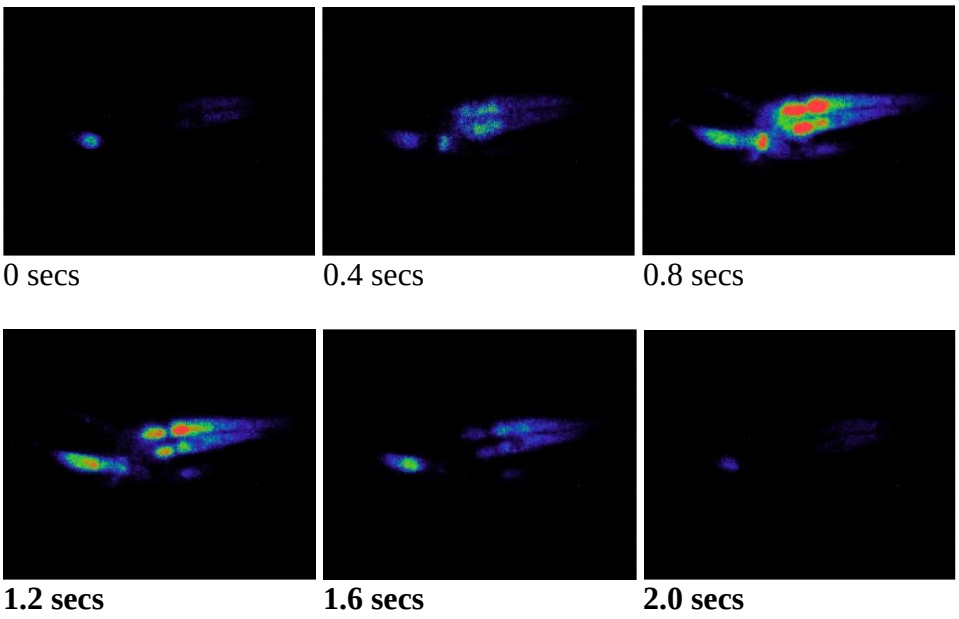

Figure 4.9 Pseudo-color intensity time frame images of intracellular calcium ion flux stained using fluo-4-AM indicator in 2D co-culture of neonatal primary cardiomyocytes and fibroblasts cultured for 4 days. 200X original magnification

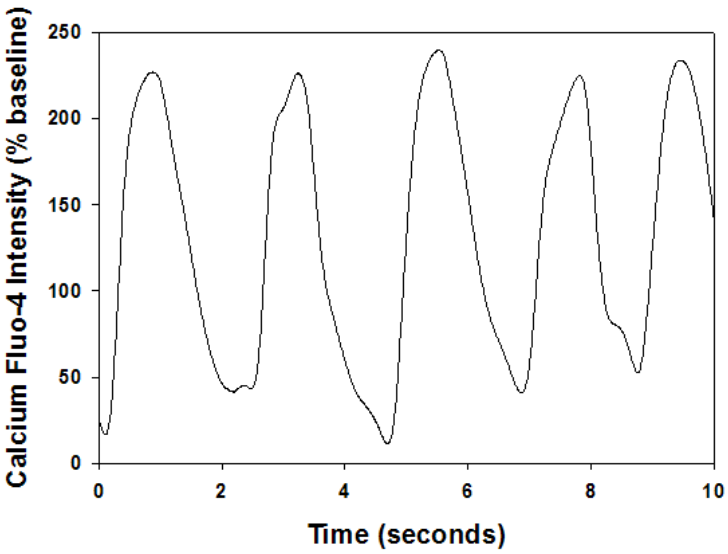

Figure 4.10 Frequency of intracellular calcium ion flux in the 2D co-culture of neonatal primary cardiomyocytes and fibroblasts after 4 days in culture.

Figure 4.11 shows the pseudo color time-frame images of the 3-D cardiomyocyte-fibroblast co-culture system. The image analysis of the calcium flux resulted in a frequency of 17 ± 3 contractions per minute.

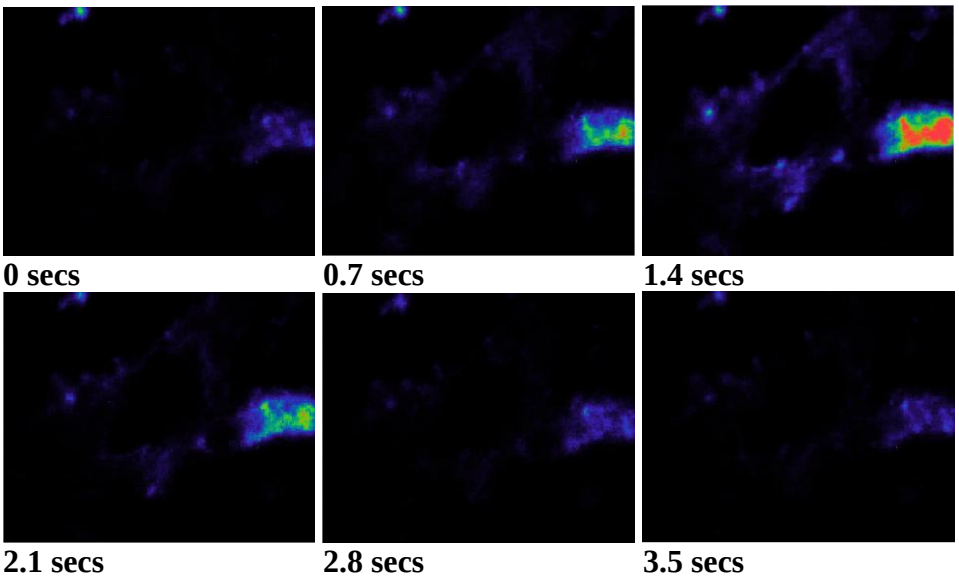

Figure 4.11 Pseudo-color intensity time frame images of intracellular calcium ion flux stained using fluo-4-AM indicator in 3D co-culture of neonatal primary cardiomyocytes and fibroblasts cultured for 7days. 200X original magnification

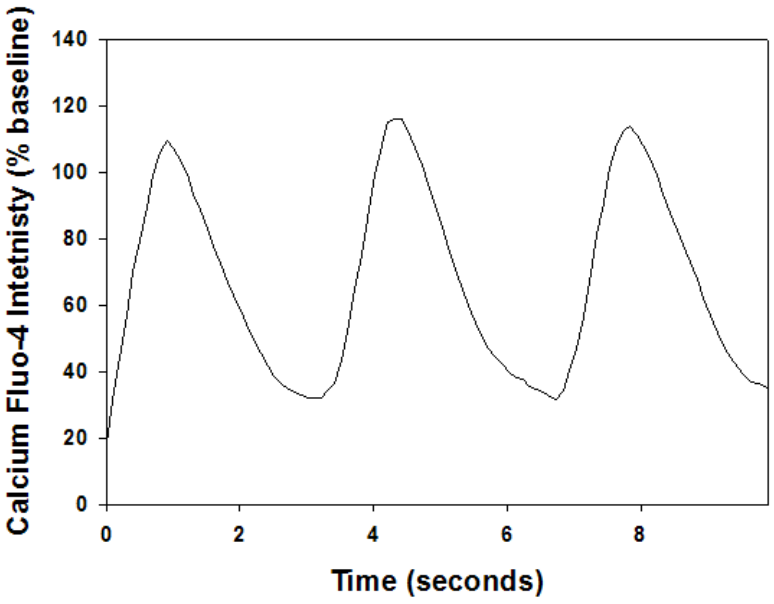

Figure 4.12 Frequency of intracellular calcium ion flux in the 3D co-culture of neonatal primary cardiomyocytes and fibroblasts after 7 days in culture.

Figure 4.13 shows the pseudo color time-frame images of the 3-D triculture endothelial cell vascularized cardiomyocyte-fibroblast system. The image analysis of the calcium flux resulted in a frequency of 28 ± 3 contractions per minute.

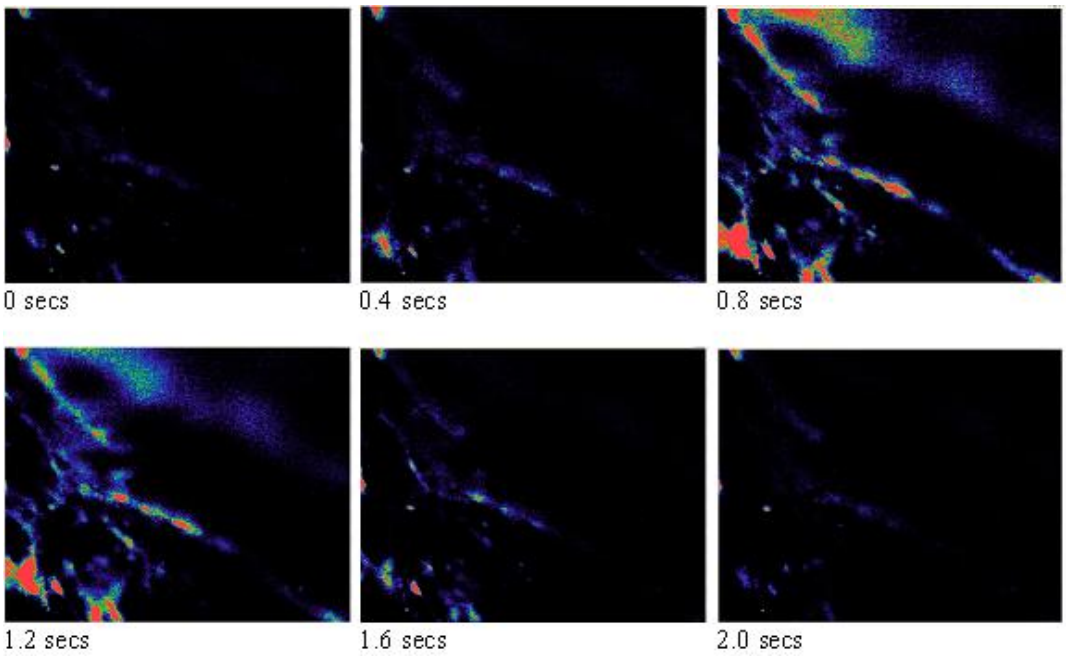

Figure 4.13 Pseudo-color intensity time frame images of intracellular calcium ion flow in 3D tri-culture system of endothelial cells, neonatal primary cardiomyocytes, and fibroblasts after 7 day culture, 200X original magnification

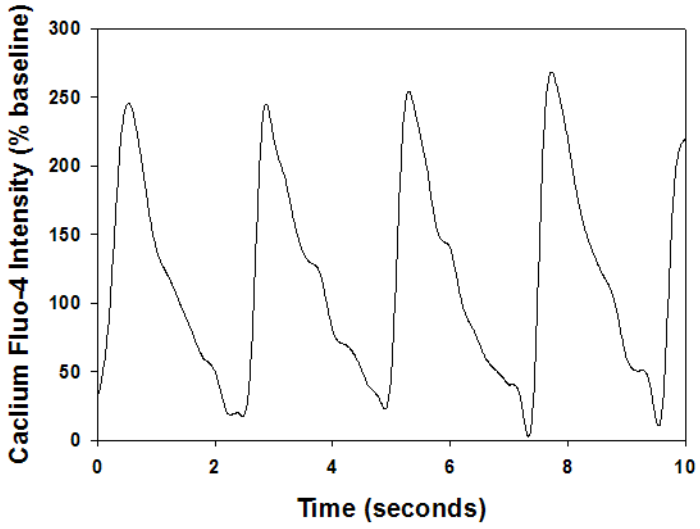

Figure 4.14 Frequency of intracellular calcium ion flux in the 3D tri-culture of endothelial cells, neonatal primary cardiomyocytes, and fibroblasts after 7 days in culture.

From the pseudo-color image analysis it is important to observe the following:

1. In the 2D cardiomyocyte-fibroblast coculture system, the cardiomyocytes attained an elongated morphology as compared to the mono-culture where the cells spread out and displayed a flattened morphology.
2. In the 3D vascularized cardiomyocyte-fibroblast tri-culture system, the cardiomyocytes formed a network of tubules that displayed rhythmic and synchronized calcium ion fluxes.

4.4 Discussion

Cardiac fibroblasts are the most abundant non-cardiomyocyte cells in the mature heart. Their functions include deposition of the extracellular matrix (ECM), paracrine signaling and propagation of the electrical stimuli. In this study, we used murine 3T3-J2 fibroblasts cell line for cardiac co-cultures because of their easy access, propagation, and high induction of epithelial cell functions (e.g. hepatocytes) [131-133]. **The key feature of the approach used in this research is the co-culturing of cardiomyocytes with fibroblasts within a vascularized 3-D scaffold for long-term functionality of the cardiomyocytes.**

To investigate the functionality and viability of cardiomyocytes, the expression of contractile alpha-sarcomeric actin (SA) and cardiomyocyte gap junction protein connexin-43 (Cx43) was used. SA-actin expression is solely found in cardiomyocytes and is an indicative sign of cardiomyocyte functional maturity. Cx43 is the gap junction protein that is mainly found in ventricular cardiomyocytes [134]. The Cx43 mediates fibroblasts heterogeneous coupling, such as between cardiomyocytes and fibroblasts [135]. These gap junctions with fibroblasts are known to propagate electrical stimuli for 100 μm [134]. The results from both the 2-D and 3-D cultures indicate that fibroblasts co-cultures resulted in the highest levels of SA-actin and Cx43 expression, suggesting fibroblasts are essential in maintaining cardiomyocytes viability and function in vitro.

The observed cardiomyocyte co-culture enhancement effect can be attributed to many of the fibroblasts' physiological functions in the native heart. Fibroblasts which constitute 70% of the normal adult heart regulate the mechanical stability and structural integrity of the cardiomyocytes via the dynamic generation of the extracellular matrix and its turnover. From a histological view point, the myocytes laminae are enclosed in a

network of endomysial collagen maintained by the fibroblasts [136]. Recent studies have observed that the extracellular matrix produced by the fibroblasts maintain Cx43 since it is regulated by heparin binding-epidermal growth factor (EGF) [137]. Hence, the results demonstrate that fibroblasts should be an integral part of any cardiac regenerative therapy as its role in providing a cardiomyocyte-compatible scaffold is of supreme importance.

The tubulogenesis of the endothelial cells on the chitosan scaffold recreates the rich vasculature architecture that perfuses the native myocardial tissue. This technology can be used as a platform to induce vascularization of various tissue regeneration constructs or to build in vitro tissue models. The fact that cardiomyocytes are able to survive and contract on chitosan nanofibers mats has never been reported before, to our knowledge.

To assess cardiomyocyte contractility, transient calcium ion staining was performed. Calcium is the most important ion involved in the excitation-contraction coupling in cardiomyocytes. Briefly, for contraction to occur, intracellular calcium ion concentration increases as calcium enters via depolarization-activated calcium transmembrane channels. This flux of calcium ions initiate the release of more calcium that is sequestered in the sarcoplasmic reticulum, Figure 4.15. The calcium binds to the thin-filamentous protein troponinC which cooperatively activates the myofilaments initiating contraction. For relaxation to occur, the intracellular calcium ions are depleted via SR Ca-ATPase, Na/Ca exchange, Ca ATPase and mitochondrial Ca uniport [138]. Hence, intracellular calcium ion is a great method to assess cardiomyocyte functionality since it is a vital regulator of cardiomyocyte contraction.

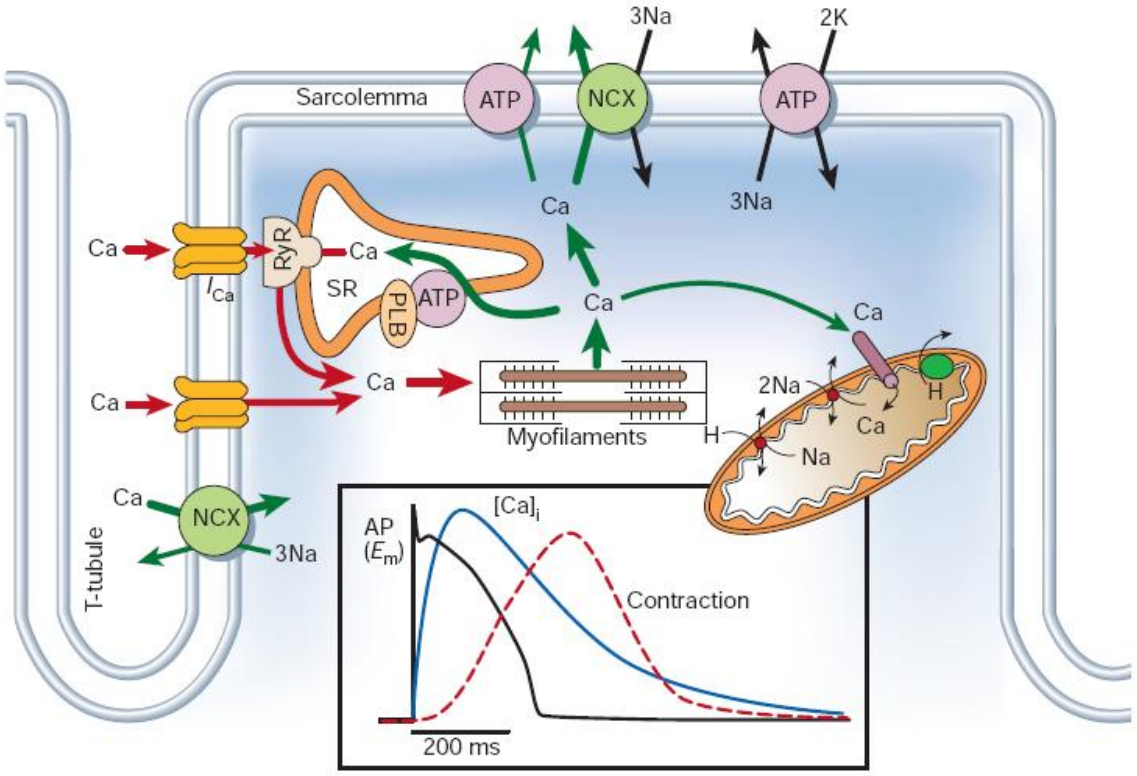

Figure 4.15 The transport of calcium ions in ventricular myocytes. The inset graph depicts the time course of a cardiomyocyte action potential, Ca ion transient concentration and cardiomyocyte contraction in a rabbit ventricular myocyte at 37°C. NCX: Na/Ca exchange; ATP: ATPase; PLB: phospholamban; SR: sarcoplasmic reticulum (Image from Bers, 2002 [138])

The monoculture of cardiomyocytes on 2D lost their functionality and their polarized morphology after 4 days. This is evident by the slow bursts of transient calcium seen in the monocultures. The co-culture system with fibroblasts demonstrated how the fibroblasts induce elongated cardiomyocyte morphology and a more rhythmic and more frequent changes in intracellular calcium ion concentrations. The most important data set is the cardiomyocyte-fibroblasts co-culture in the vascularized chitosan nanofibrous scaffolds. It is clear that the cardiomyocytes have migrated and organized themselves into myocyte tubules. The calcium flux in these elongated cardiomyocyte tubules is

synchronized and have a periodicity that is established throughout the cardiomyocyte tubular networks.

4.5 Conclusion

Results of this section of the research demonstrate that chitosan nanofibers can be used as scaffolds for the development of 3-D cardiac tissue constructs. Primary neonatal cardiomyocytes lost their viability and functionality in vitro when cultured alone. The cardiac-fibroblasts co-culture model is a promising system for the maintenance of long-term survival and functionality of cardiomyocytes in vitro. The fibroblast co-culture system also induces the cardiomyocytes to increase gap junction expression and attain tubular morphology. These modifications in the cardiomyocytes encourage the cells to function in syncytium as a 3D cardiac tissue model.

CHAPTER 5

SUMMARY AND FUTURE STUDIES

The essence of this research endeavor was to create a cardiac tissue model. The avenue pursued to reach this goal focused on recreating, as close as possible, the acellular and cellular components of the cardiomyocyte in vivo cellular niche. The natural acellular components include but are not limited to the collagen nanofiber scaffold and the glycosaminoglycan hydrogel milieu. The natural cardiac cellular mosaic is mainly composed of the dense endothelial cell vasculature bed that perfuses a cardiomyocyte: fibroblast co-culture. In other words, the design inputs for the acellular and cellular components of the engineered cardiac tissue model were dictated by the natural cardiac tissue itself.

To satisfy the acellular design inputs, chitosan a cheap, non-toxic, biodegradable and naturally derived polysaccharide was electrospun into nanofibers to recreate the collagen nanofiber matrix. In addition, chitosan shares structural homology with the glycosaminoglycans of the natural extracellular matrix. Therefore, the electrospun chitosan nanofiber scaffold combined the physical collagenous nanofibrous architecture with the structural glycosaminoglycan functionality into one scaffold.

To recreate the myocardial cellular mosaic, the chitosan nanofibers were impregnated with endothelial cells and cultured for a week to allow the formation of a network of endothelial tubes resembling the myocardial vasculature bed. The mechanism of tubulogenesis induction by the fibronectin adsorbed chitosan nanofibers need further detailed characterization. The extracellular matrix plays a critical role in synchronizing

the signals that control angiogenesis. The literature provides evidence that suggests that the extracellular matrix balances vascular morphogenesis and vascular regression as shown in figure 5.1. Furthermore, integrin signal transduction pathways involving the activation of Cdc42 and Rac1 initiate critical downstream signaling molecules that control endothelial cell tube morphogenesis [139].

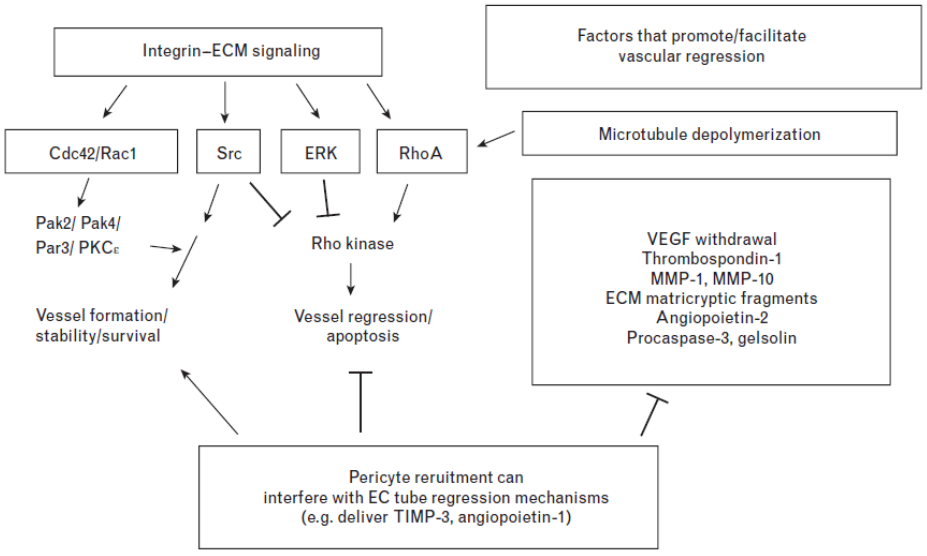

Figure 5.1 The genes and signaling pathways that are involved in the regulation of vascular morphogenesis/regression balance.

More specifically, there are a number of published results that point to the vital role of fibronectin receptors, α5β1, α4β1, and α9β1 in endothelial morphogenesis in the formation of blood vessels [140]. Knocking out fibronectin or the integrin α5 subunit results in substantial defects in the vascular phenotypes, pointing toward the essential role of the fibronectin-integrin ligand/receptor interaction in vascularization [141]. An interesting study to conduct would be the splicing of the fibronectin protein into smaller peptide sequences to determine which particular sequence is involved in the induction of vascular morphogenesis.

In addition to fibronectin, the induction of endothelial tubulogenesis and activation can be initiated via multiple extracellular matrix components such as different types of collagens and fibrin matrices which have been shown to increase the production of F-actin stress fibers and the disruption of VE-cadherin intercellular junction proteins resulting in endothelial morphogenesis into tubules. On the other hand as seen in figure 5.2, laminin which is another component of the extracellular matrix does not induce the formation of stress fibers and VE-cadherin intercellular junctions remain intact [142].

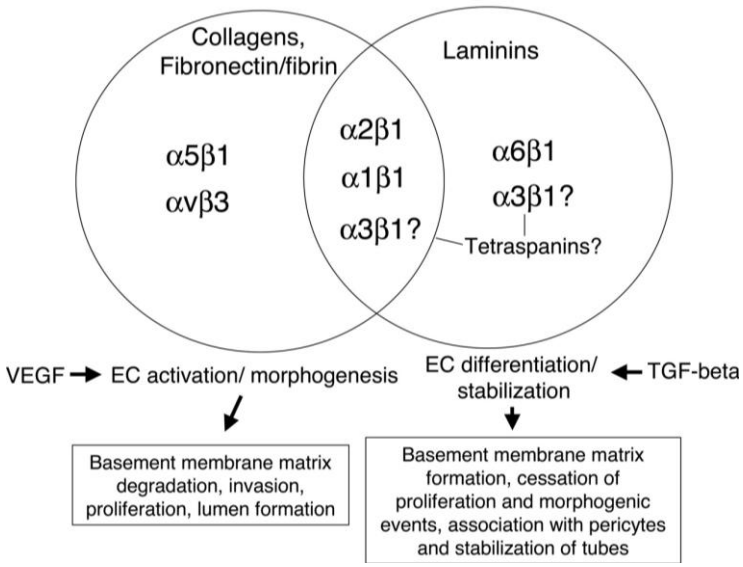

Figure 5.2 The effect of collagen type I, fibronectin,/fibrin, and lamini-1 on endothelial tubulogenesis. The activation of Src and Rho signaling pathways and suppression of Rac and PKA via collagen and fibronectin/fibrin interaction with α5β1 and αvβ3 integrin receptors leads to the formation of actin stress fibers, the dissociation of the intercellular junction proteins VE-cadherin and the tubular morphogenesis. However, laminin has the effect of stopping endothelial morphogenic events and the stabilization of the tubules via pericytes recruitment [142].

The cardiomyocytes and fibroblasts were then seeded onto the vascularized chitosan scaffold to fully recapitulate the cellular composition of the myocardium. The results clearly show that the vascularized cardiomyocyte-fibroblasts system have induced the cardiomyocytes to communicate with each other to enable the formation of a network

of cardiomyocyte tubules that function in syncytium. This research demonstrates the importance of the fibroblasts co-culture in maintaining the functionality of primary cardiomyocytes in vitro for up to four weeks; a requirement for any useful cardiac tissue model. Furthermore, the endothelial tube formation on the chitosan nanofibers can be used as a platform technology to provide vasculature architecture for numerous tissue models.

There are a number of studies that show evidence of the pro-inflammatory responses of chitosan as it attracts and activates macrophages. Feng et al. demonstrated that oligochitosan (less than 10 saccharide residues) can be internalized by macrophages via lectin receptors with mannose specificity [143]. Consequently, chitosan has a stimulatory effect on the secretion of tumor necrosis factor-α, interleukin-1 β, macrophage colony stimulating factor (GM-CSF), nitric oxide (NO), and interleukin-6 in macrophages [144]. Huang et al. attributes chitosan's inflammatory response to its cationic polyelectrolyte properties in attracting and activating macrophages [145]. This is due to the finding that cationic groups cause irreversible and strong cell adhesion invoking a strong inflammatory response [146]. These inflammatory responses can be controlled by varying the degree of deacetylation of the chitosan being used or by incorporating immune-modulating cells such as mesenchymal stem cells [147, 148].

The cardiac tissue model developed in this research showed promising results in terms of attaining cardiomyocyte tubular morphology, synchronized contractility, and a network of tubular endothelial cells. Future studies should focus on:

1. Building a mechanical stimulation bioreactor to condition the cardiac tissue model with physiological loading.

2. Assessing the swelling and stability of the chitosan nanofibers in human plasma.
3. Assessing the engraftment of the cardiac patch with in vivo animal studies.
4. Studying the pharmacology of cardiac drugs on the cardiac patch to determine its feasibility as a diagnostics tool or drug screening tissue platform.
5. Examining cross-sections of the tissue-model to assess the migration and infiltration of the cellular constructions within the scaffold. This can be done by cryogenic freezing of the tissue-model and then cross-sectioning them into pieces for histological staining. Another method would be the used of confocal microscopy to examine the vertical planes of tissue-model
6. More detailed examination of the calcium ion staining to understand the cellular functioning and how it correlates with certain features or shoulders of the calcium ion wave.
7. Study why the xenogeneic tissue model allows the cardiomyocyte to maintain functionality and viability.

In conclusion, this research has shown “proof-of-concept” of maintaining primary cardiomyocyte viability and inducing tubular and tissue-like contractility via the recreation of the acellular and cellular cardiomyocyte niche.

REFERENCES

1. Chen, Q., et al., *Biomaterials in cardiac tissue engineering: Ten years of research survey.* Materials Science and Engineering: R: Reports, 2008. **59**(1-6): p. 1-37.

2. Anversa, P., et al., *Ischaemic myocardial injury and ventricular remodelling.* Cardiovascular research, 1993. **27**(2): p. 145.

3. Sutton, M.G. and N. Sharpe, *Left ventricular remodeling after myocardial infarction: pathophysiology and therapy.* Circulation, 2000. **101**(25): p. 2981.

4. Baig, M., et al., *The pathophysiology of advanced heart failure.* American Heart Journal, 1998. **135**(6): p. S216-S230.

5. Soonpaa, M.H. and L.J. Field, *Survey of studies examining mammalian cardiomyocyte DNA synthesis.* Circulation research, 1998. **83**(1): p. 15.

6. Miner, E.C. and W.L. Miller. *A look between the cardiomyocytes: the extracellular matrix in heart failure*. 2006: Mayo Clinic.

7. Martinez, C., et al., *Pacemakers and defibrillators: recent and ongoing studies that impact the elderly.* The American Journal of Geriatric Cardiology, 2007. **15**(2): p. 82-87.

8. Packer, M., *The impossible task of developing a new treatment for heart failure.* Journal of Cardiac Failure, 2002. **8**(4): p. 193-196.

9. Koh, G., et al., *Differentiation and long-term survival of C2C12 myoblast grafts in heart.* Journal of Clinical Investigation, 1993. **92**(3): p. 1548.

10. Koh, G., et al., *Long-term survival of AT-1 cardiomyocyte grafts in syngeneic myocardium.* American Journal of Physiology- Heart and Circulatory Physiology, 1993. **264**(5): p. H1727.

11. Soonpaa, M., et al., *Formation of nascent intercalated disks between grafted fetal cardiomyocytes and host myocardium.* Science, 1994. **264**(5155): p. 98.

12. Menasche, P., et al., *Autologous skeletal myoblast transplantation for severe postinfarction left ventricular dysfunction* 1.* Journal of the American College of Cardiology, 2003. **41**(7): p. 1078-1083.

13. Christman, K.L. and R.J. Lee, *Biomaterials for the treatment of myocardial infarction.* Journal of the American College of Cardiology, 2006. **48**(5): p. 907-913.

14. Wang, F. and J. Guan, *Cellular cardiomyoplasty and cardiac tissue engineering for myocardial therapy.* Advanced Drug Delivery Reviews, 2010. **62**(7-8): p. 784-797.

15. Gomes Pessanha, M. and C.A. Mandarim-de-Lacerda, *Influence of the chronic nitric oxide synthesis inhibition on cardiomyocytes number.* Virchows Archiv, 2000. **437**(6): p. 667-674.

16. Giraud, M.N., et al., *Current state of the art in myocardial tissue engineering.* Tissue Engineering, 2007. **13**(8): p. 1825-1836.

17. Chen, Q.-Z., et al., *Characterisation of a soft elastomer poly(glycerol sebacate) designed to match the mechanical properties of myocardial tissue.* Biomaterials, 2008. **29**(1): p. 47-57.

18. Zimmermann, W.H., et al., *Engineered heart tissue grafts improve systolic and diastolic function in infarcted rat hearts.* Nature medicine, 2006. **12**(4): p. 452-458.

19. Zimmermann, W., et al., *Tissue engineering of a differentiated cardiac muscle construct.* Circulation research, 2002. **90**(2): p. 223.

20. Leor, J., et al., *Bioengineered cardiac grafts: A new approach to repair the infarcted myocardium?* Circulation, 2000. **102**(90003).

21. Shimizu, T., et al., *Cell sheet engineering for myocardial tissue reconstruction.* Biomaterials, 2003. **24**(13): p. 2309-2316.

22. Shimizu, T., et al., *Fabrication of pulsatile cardiac tissue grafts using a novel 3-dimensional cell sheet manipulation technique and temperature-responsive cell culture surfaces.* Circulation research, 2002. **90**(3): p. e40.

23. Anderson, J.M., A. Rodriguez, and D.T. Chang, *Foreign body reaction to biomaterials.* Seminars in Immunology, 2008. **20**(2): p. 86-100.

24. Nair, L.S. and C.T. Laurencin, *Biodegradable polymers as biomaterials.* Progress in Polymer Science. **32**(8-9): p. 762-798.

25. Aebischer, P., et al., *Piezoelectric guidance channels enhance regeneration in the mouse sciatic nerve after axotomy.* Brain research, 1987. **436**(1): p. 165-168.

26. Schmidt, C.E. and J.B. Leach, *Neural tissue engineering: strategies for repair and regeneration.* Biomedical Engineering, 2003. **5**.

27. Schmidt, C.E., et al., *Stimulation of neurite outgrowth using an electrically conducting polymer.* Proceedings of the National Academy of Sciences of the United States of America, 1997. **94**(17): p. 8948.

28. MacNeil, S., *Biomaterials for tissue engineering of skin.* Materials Today, 2008. **11**(5): p. 26-35.

29. Jayakumar, R., et al., *Novel chitin and chitosan nanofibers in biomedical applications.* Biotechnol Adv, 2010. **28**(1): p. 142-50.

30. Choi, C.Y., et al., *Effect of N-acylation on structure and properties of chitosan fibers.* Carbohydrate Polymers, 2007. **68**(1): p. 122-127.

31. Jaworska, M., et al., *Influence of chitosan characteristics on polymer properties. I: Crystallographic properties.* Polymer International, 2003. **52**(2): p. 198-205.

32. Pillai, C.K.S., W. Paul, and C.P. Sharma, *Chitin and chitosan polymers: Chemistry, solubility and fiber formation.* Progress in Polymer Science, 2009. **34**(7): p. 641-678.

33. Sarasam, A. and S.V. Madihally, *Characterization of chitosan-polycaprolactone blends for tissue engineering applications.* Biomaterials, 2005. **26**(27): p. 5500-5508.

34. Francis Suh, J.K. and H.W.T. Matthew, *Application of chitosan-based polysaccharide biomaterials in cartilage tissue engineering: a review.* Biomaterials, 2000. **21**(24): p. 2589-2598.

35. Adekogbe, I. and A. Ghanem, *Fabrication and characterization of DTBP-crosslinked chitosan scaffolds for skin tissue engineering.* Biomaterials, 2005. **26**(35): p. 7241-7250.

36. Amaral, I., et al., *Rat bone marrow stromal cell osteogenic differentiation and fibronectin adsorption on chitosan membranes: The effect of the degree of acetylation.* Journal of Biomedical Materials Research Part A, 2005. **75**(2): p. 387.

37. Haipeng, G., et al., *Studies on nerve cell affinity of chitosan-derived materials.* Journal of biomedical materials research, 2000. **52**(2): p. 285-295.

38. Sui, R., et al., *The Current Status of Engineering Myocardial Tissue.* Stem Cell Reviews and Reports, 2010: p. 1-9.

39. Akhyari, P., et al., *Mechanical stretch regimen enhances the formation of bioengineered autologous cardiac muscle grafts.* Circulation, 2002. **106**(90121).

40. Kofidis, T., et al., *Novel injectable bioartificial tissue facilitates targeted, less invasive, large-scale tissue restoration on the beating heart after myocardial injury.* Circulation, 2005. **112**(9_suppl).

41. Kofidis, T., et al., *In vitro engineering of heart muscle: artificial myocardial tissue.* The Journal of Thoracic and Cardiovascular Surgery, 2002. **124**(1): p. 63.

42. Christman, K.L., et al., *Fibrin glue alone and skeletal myoblasts in a fibrin scaffold preserve cardiac function after myocardial infarction.* Tissue Engineering, 2004. **10**(3-4): p. 403-409.

43. Eschenhagen, T., et al., *Three-dimensional reconstitution of embryonic cardiomyocytes in a collagen matrix: a new heart muscle model system.* The FASEB Journal, 1997. **11**(8): p. 683.

44. Eschenhagen, T., et al., *3D engineered heart tissue for replacement therapy.* Basic Research in Cardiology, 2002. **97**(7).

45. Ke, Q., et al., *Embryonic stem cells cultured in biodegradable scaffold repair infarcted myocardium in mice.* Acta Physiologica Sinica, 2005. **57**(6): p. 673-681.

46. Bursac, N., et al., *Cardiac muscle tissue engineering: toward an in vitro model for electrophysiological studies.* American Journal of Physiology- Heart and Circulatory Physiology, 1999. **277**(2): p. H433.

47. Engelmayr, G.C., et al., *Accordion-like honeycombs for tissue engineering of cardiac anisotropy.* Nature materials, 2008. **7**(12): p. 1003-1010.

48. Piao, H., et al., *Effects of cardiac patches engineered with bone marrow-derived mononuclear cells and PGCL scaffolds in a rat myocardial infarction model.* Biomaterials, 2007. **28**(4): p. 641-649.

49. McDevitt, T.C., et al., *Spatially organized layers of cardiomyocytes on biodegradable polyurethane films for myocardial repair.* Journal of Biomedical Materials Research Part A, 2003. **66**(3): p. 586-595.

50. Christman, K.L., et al., *Injectable fibrin scaffold improves cell transplant survival, reduces infarct expansion, and induces neovasculature formation in ischemic myocardium.* Journal of the American College of Cardiology, 2004. **44**(3): p. 654-660.

51. Boerboom, R.A., et al., *Effect of strain magnitude on the tissue properties of engineered cardiovascular constructs.* Annals of Biomedical Engineering, 2008. **36**(2): p. 244-253.

52. Bissell, M.J., H.G. Hall, and G. Parry, *How does the extracellular matrix direct gene expression?* Journal of Theoretical Biology, 1982. **99**(1): p. 31-68.

53. Owen, S.C. and M.S. Shoichet, *Design of three dimensional biomimetic scaffolds.* Journal of Biomedical Materials Research Part A. **94**(4): p. 1321-1331.

54. Guo, W. and F.G. Giancotti, *Integrin signalling during tumour progression.* Nature Reviews Molecular Cell Biology, 2004. **5**(10): p. 816-826.

55. Vlodavsky, I., et al., *Extracellular sequestration and release of fibroblast growth factor: a regulatory mechanism?* Trends in Biochemical Sciences, 1991. **16**: p. 268-271.

56. Li, S., et al., *Matrix assembly, regulation, and survival functions of laminin and its receptors in embryonic stem cell differentiation.* The Journal of cell biology, 2002. **157**(7): p. 1279.

57. Wang, N. and D.E. Ingber, *Control of cytoskeletal mechanics by extracellular matrix, cell shape, and mechanical tension.* Biophysical Journal, 1994. **66**(6): p. 2181-2189.

58. Hagios, C., A. Lochter, and M.J. Bissell, *Tissue architecture: the ultimate regulator of epithelial function?* Philosophical Transactions of the Royal Society B: Biological Sciences, 1998. **353**(1370): p. 857.

59. Délot, E.C., *Control of endocardial cushion and cardiac valve maturation by BMP signaling pathways.* Molecular genetics and metabolism, 2003. **80**(1-2): p. 27-35.

60. Weber, K.T., *From inflammation to fibrosis: a stiff stretch of highway.* Hypertension, 2004. **43**(4): p. 716.

61. Eschenhagen, T. and W.H. Zimmermann, *Engineering myocardial tissue.* Circulation research, 2005. **97**(12): p. 1220.

62. Makino, S., et al., *Cardiomyocytes can be generated from marrow stromal cells in vitro.* Journal of clinical investigation, 1999. **103**(5): p. 697-705.

63. Badorff, C., et al., *Transdifferentiation of blood-derived human adult endothelial progenitor cells into functionally active cardiomyocytes.* Circulation, 2003. **107**(7): p. 1024.

64. Condorelli, G., et al., *Cardiomyocytes induce endothelial cells to trans-differentiate into cardiac muscle: implications for myocardium regeneration.* Proceedings of the National Academy of Sciences of the United States of America, 2001. **98**(19): p. 10733.

65. Huang, J., et al., *Multilineage cells from human adipose tissue: implications for cell-based therapies.* Tissue Engineering, 2001. **7**(2).

66. Beltrami, A.P., et al., *Adult cardiac stem cells are multipotent and support myocardial regeneration.* Cell, 2003. **114**(6): p. 763-776.

67. Kehat, I., et al., *Human embryonic stem cells can differentiate into myocytes with structural and functional properties of cardiomyocytes.* Journal of clinical investigation, 2001. **108**(3): p. 407-414.

68. Sill, T.J. and H.A. von Recum, *Electrospinning: Applications in drug delivery and tissue engineering.* Biomaterials, 2008. **29**(13): p. 1989-2006.

69. Ohkawa, K., et al., *Electrospinning of chitosan.* Macromolecular Rapid Communications, 2004. **25**(18): p. 1600-1605.

70. Min, B.M., et al., *Chitin and chitosan nanofibers: electrospinning of chitin and deacetylation of chitin nanofibers.* Polymer, 2004. **45**(21): p. 7137-7142.

71. Senel, S. and S.J. McClure, *Potential applications of chitosan in veterinary medicine.* Advanced Drug Delivery Reviews, 2004. **56**(10): p. 1467-1480.

72. Geng, X., O.H. Kwon, and J. Jang, *Electrospinning of chitosan dissolved in concentrated acetic acid solution.* Biomaterials, 2005. **26**(27): p. 5427-5432.

73. Sangsanoh, P. and P. Supaphol, *Stability improvement of electrospun chitosan nanofibrous membranes in neutral or weak basic aqueous solutions.* Biomacromolecules, 2006. **7**(10): p. 2710-2714.

74. Bhattarai, N., et al., *Electrospun chitosan-based nanofibers and their cellular compatibility.* Biomaterials, 2005. **26**(31): p. 6176-6184.

75. Neamnark, A., R. Rujiravanit, and P. Supaphol, *Electrospinning of hexanoyl chitosan.* Carbohydrate Polymers, 2006. **66**(3): p. 298-305.

76. Hasegawa, M., et al., *Dissolving states of cellulose and chitosan in trifluoroacetic acid.* Journal of Applied Polymer Science, 1992. **45**(10): p. 1857-1863.

77. Knill, C.J., et al., *Acid hydrolysis of commercial chitosans.* Journal of Chemical Technology & Biotechnology, 2005. **80**(11): p. 1291-1296.

78. Jayakumar, R., et al., *Biomaterials based on chitin and chitosan in wound dressing applications.* Biotechnology Advances. **In Press, Uncorrected Proof**.

79. Kittur, F., et al., *Chitooligosaccharides--preparation with the aid of pectinase isozyme from Aspergillus niger and their antibacterial activity.* Carbohydrate Research, 2005. **340**(6): p. 1239-1245.

80. Kulish, E., et al., *Enzymatic degradation of chitosan films by collagenase.* Polymer Science Series B, 2006. **48**(5): p. 244-246.

81. Vårum, K.M., et al., *In vitro degradation rates of partially N-acetylated chitosans in human serum.* Carbohydrate Research, 1997. **299**(1-2): p. 99-101.

82. Freier, T., et al., *Controlling cell adhesion and degradation of chitosan films by N-acetylation.* Biomaterials, 2005. **26**(29): p. 5872-5878.

83. Pangburn, S.H., P.V. Trescony, and J. Heller, *Lysozyme degradation of partially deacetylated chitin, its films and hydrogels.* Biomaterials, 1982. **3**(2): p. 105-108.

84. Balau, L., et al., *Physico-chemical properties of chitosan films.* Central European Journal of Chemistry, 2004. **2**(4): p. 638-647.

85. Cervera, M.F., et al., *Solid-state characterization of chitosans derived from lobster chitin.* Carbohydrate Polymers, 2004. **58**(4): p. 401-408.

86. Cervera, M., et al., *Solid-state characterization of chitosans derived from lobster chitin.* Carbohydrate Polymers, 2004. **58**(4): p. 401-408.

87. Hynes, R.O., *Integrins: Bidirectional, Allosteric Signaling Machines.* Cell, 2002. **110**(6): p. 673-687.

88. Geiger, B., et al., *Transmembrane crosstalk between the extracellular matrix and the cytoskeleton.* Nature Reviews Molecular Cell Biology, 2001. **2**(11): p. 793-805.

89. Deligianni, D.D., et al., *Effect of surface roughness of hydroxyapatite on human bone marrow cell adhesion, proliferation, differentiation and detachment strength.* Biomaterials, 2001. **22**(1): p. 87-96.

90. Young, B.R., W.G. Pitt, and S.L. Cooper, *Protein adsorption on polymeric biomaterials I. Adsorption isotherms.* Journal of Colloid and Interface Science, 1988. **124**(1): p. 28-43.

91. Chou, L., B. Marek, and W. Wagner, *Effects of hydroxylapatite coating crystallinity on biosolubility, cell attachment efficiency and proliferation in vitro.* Biomaterials, 1999. **20**(10): p. 977-985.

92. Hallab, N., et al., *Cell adhesion to biomaterials: correlations between surface charge, surface roughness, adsorbed protein, and cell morphology.* Journal of long-term effects of medical implants, 1995. **5**(3): p. 209.

93. Kleinman, H.K. and G.R. Martin, *Matrigel: Basement membrane matrix with biological activity.* Seminars in Cancer Biology, 2005. **15**(5): p. 378-386.

94. Engbring, J.A. and H.K. Kleinman, *The basement membrane matrix in malignancy.* The Journal of Pathology, 2003. **200**(4): p. 465-470.

95. Rouwkema, J., N. Rivron, and C. van Blitterswijk, *Vascularization in tissue engineering.* Trends in Biotechnology, 2008. **26**(8): p. 434-441.

96. Hsieh, P., et al., *Endothelial-cardiomyocyte interactions in cardiac development and repair.* 2006.

97. Caspi, O., et al., *Tissue engineering of vascularized cardiac muscle from human embryonic stem cells.* Circulation research, 2007. **100**(2): p. 263-272.

98. Zhao, Y., et al., *Neuregulins promote survival and growth of cardiac myocytes.* Journal of Biological Chemistry, 1998. **273**(17): p. 10261.

99. Kuramochi, Y., et al., *Cardiac endothelial cells regulate reactive oxygen species-induced cardiomyocyte apoptosis through neuregulin-1 /erbB4 signaling.* Journal of Biological Chemistry, 2004. **279**(49): p. 51141.

100. Lemmens, K., et al., *Neuregulin-1 induces a negative inotropic effect in cardiac muscle: role of nitric oxide synthase.* Circulation, 2004. **109**(3): p. 324.

101. Rich, S. and V. McLaughlin, *Endothelin receptor blockers in cardiovascular disease.* Circulation, 2003. **108**(18): p. 2184.

102. Hoch, R. and P. Soriano, *Roles of PDGF in animal development.* Development, 2003. **130**(20): p. 4769.

103. Chiu, L. and M. Radisic, *Scaffolds with covalently immobilized VEGF and Angiopoietin-1 for vascularization of engineered tissues.* Biomaterials, 2009.

104. Asakawa, N., et al., *Pre-vascularization of in vitro three-dimensional tissues created by cell sheet engineering.* Biomaterials.

105. Dvir, T., et al., *Prevascularization of cardiac patch on the omentum improves its therapeutic outcome.* Proceedings of the National Academy of Sciences, 2009. **106**(35): p. 14990.

106. Aoki, H., S. Izumo, and J. Sadoshima, *Angiotensin II activates RhoA in cardiac myocytes: a critical role of RhoA in angiotensin II-induced premyofibril formation.* Circ Res, 1998. **82**(6): p. 666-76.

107. Keselowsky, B.G., D.M. Collard, and A.J. García, *Surface chemistry modulates fibronectin conformation and directs integrin binding and specificity to control cell adhesion.* Journal of Biomedical Materials Research Part A, 2003. **66A**(2): p. 247-259.

108. Arnaoutova, I., et al., *The endothelial cell tube formation assay on basement membrane turns 20: state of the science and the art.* Angiogenesis, 2009. **12**(3): p. 267-274.

109. Grant, D.S., et al., *Two different laminin domains mediate the differentiation of human endothelial cells into capillary-like structures in vitro.* Cell, 1989. **58**(5): p. 933-943.

110. Vernon, R., et al., *Reorganization of basement membrane matrices by cellular traction promotes the formation of cellular networks in vitro.* Laboratory investigation; a journal of technical methods and pathology, 1992. **66**(5): p. 536.

111. Davis, G. and D. Senger, *Endothelial extracellular matrix: biosynthesis, remodeling, and functions during vascular morphogenesis and neovessel stabilization.* Circulation research, 2005. **97**(11): p. 1093.

112. Giancotti, F.G. and E. Ruoslahti, *Integrin Signaling.* Science, 1999. **285**(5430): p. 1028-1033.

113. Riveline, D., et al., *Focal contacts as mechanosensors: externally applied local mechanical force induces growth of focal contacts by an mDia1-dependent and ROCK-independent mechanism.* Science's STKE, 2001. **153**(6): p. 1175.

114. Burridge, K., *Substrate adhesions in normal and transformed fibroblasts: organization and regulation of cytoskeletal, membrane and extracellular matrix components at focal contacts.* Cancer Rev, 1986. **4**: p. 18-78.

115. Vliegen, H., et al., *Myocardial changes in pressure overload-induced left ventricular hypertrophy: A study on tissue composition, polyploidization and multinucleation.* European heart journal, 1991. **12**(4): p. 488.

116. Nag, A., *Study of non-muscle cells of the adult mammalian heart: a fine structural analysis and distribution.* Cytobios, 1980. **28**(109): p. 41.

117. Parker, K. and D. Ingber, *Extracellular matrix, mechanotransduction and structural hierarchies in heart tissue engineering.* Philosophical Transactions of the Royal Society B: Biological Sciences, 2007. **362**(1484): p. 1267.

118. Camelliti, P., T. Borg, and P. Kohl, *Structural and functional characterisation of cardiac fibroblasts.* Cardiovascular research, 2005. **65**(1): p. 40.

119. Baudino, T.A., et al., *Cardiac fibroblasts: friend or foe?* American Journal of Physiology-Heart and Circulatory Physiology, 2006. **291**(3): p. H1015.

120. Bowers, S.L.K., I. Banerjee, and T.A. Baudino, *The extracellular matrix: at the center of it all.* Journal of Molecular and Cellular Cardiology. **48**(3): p. 474-482.

121. Manabe, I., T. Shindo, and R. Nagai, *Gene expression in fibroblasts and fibrosis: involvement in cardiac hypertrophy.* Circulation research, 2002. **91**(12): p. 1103.

122. Spinale, F., *Matrix metalloproteinases: regulation and dysregulation in the failing heart.* Circulation research, 2002. **90**(5): p. 520.

123. Gaudesius, G., et al., *Coupling of cardiac electrical activity over extended distances by fibroblasts of cardiac origin.* Circulation research, 2003. **93**(5): p. 421.

124. Carver, W., et al., *Collagen expression in mechanically stimulated cardiac fibroblasts.* Circulation research, 1991. **69**(1): p. 116.

125. Kakkar, R. and R.T. Lee, *Intramyocardial fibroblast myocyte communication.* Circulation research. **106**(1): p. 47.

126. Brutsaert, D., *Cardiac endothelial-myocardial signaling: its role in cardiac growth, contractile performance, and rhythmicity.* Physiological reviews, 2003. **83**(1): p. 59.

127. Narmoneva, D., et al., *Endothelial cells promote cardiac myocyte survival and spatial reorganization: implications for cardiac regeneration.* Circulation, 2004. **110**(8): p. 962.

128. Chilton, L., W. Giles, and G. Smith, *Evidence of intercellular coupling between co-cultured adult rabbit ventricular myocytes and myofibroblasts.* The Journal of Physiology, 2007. **583**(1): p. 225.

129. Ieda, M., et al., *Cardiac Fibroblasts Regulate Myocardial Proliferation through ²1 Integrin Signaling.* 2009. **16**(2): p. 233-244.

130. Zhang, Y., et al., *Connexin43 Expression Levels Influence Intercellular Coupling and Cell Proliferation of Native Murine Cardiac Fibroblasts.* Cell Communication and Adhesion, 2008. **15**: p. 289-303.

131. Bhatia, S.N., et al., *Effect of cell-cell interactions in preservation of cellular phenotype: cocultivation of hepatocytes and nonparenchymal cells.* Faseb J, 1999. **13**(14): p. 1883-900.

132. Cho, C.H., et al., *A new technique for primary hepatocyte expansion in vitro.* Biotechnol Bioeng, 2008. **101**(2): p. 345-56.

133. Khetani, S.R., et al., *Exploring interactions between rat hepatocytes and nonparenchymal cells using gene expression profiling.* Hepatology, 2004. **40**(3): p. 545-54.

134. van Veen, T., H. van Rijen, and T. Opthof, *Cardiac gap junction channels: modulation of expression and channel properties.* Cardiovascular research, 2001. **51**(2): p. 217.

135. Snider, P., et al., *Origin of Cardiac Fibroblasts and the Role of Periostin.* Circulation research, 2009. **105**(10): p. 934.

136. Banerjee, I., et al., *Dynamic interactions between myocytes, fibroblasts, and extracellular matrix.* Ann N Y Acad Sci, 2006. **1080**: p. 76-84.

137. Yoshioka, J., et al., *Cardiomyocyte hypertrophy and degradation of connexin43 through spatially restricted autocrine/paracrine heparin-binding EGF.* Proceedings of the National Academy of Sciences of the United States of America, 2005. **102**(30): p. 10622.

138. Bers, D.M., *Cardiac excitation–contraction coupling.* Nature, 2002. **415**(6868): p. 198-205.

139. Davis, G.E. and D.R. Senger, *Extracellular matrix mediates a molecular balance between vascular morphogenesis and regression.* Current opinion in hematology, 2008. **15**(3): p. 197.

140. Hynes, R., *Cell–matrix adhesion in vascular development.* Journal of Thrombosis and Haemostasis, 2007. **5**: p. 32-40.

141. Astrof, S., D. Crowley, and R.O. Hynes, *Multiple cardiovascular defects caused by the absence of alternatively spliced segments of fibronectin.* Developmental biology, 2007. **311**(1): p. 11-24.

142. Davis, G.E. and D.R. Senger, *Endothelial extracellular matrix: biosynthesis, remodeling, and functions during vascular morphogenesis and neovessel stabilization.* Circulation research, 2005. **97**(11): p. 1093.

143. Feng, J., L. Zhao, and Q. Yu, *Receptor-mediated stimulatory effect of oligochitosan in macrophages.* Biochemical and biophysical research communications, 2004. **317**(2): p. 414-420.

144. Peluso, G., et al., *Chitosan-mediated stimulation of macrophage function.* Biomaterials, 1994. **15**(15): p. 1215-1220.

145. Huang, Y., et al., *Pulmonary inflammation caused by chitosan microparticles.* Journal of Biomedical Materials Research Part A, 2005. **75**(2): p. 283-287.

146. Kishida, A., et al., *Cell behaviour on polymer surfaces grafted with non-ionic and ionic monomers.* Biomaterials, 1991. **12**(8): p. 786-792.

147. Patel, S.A., et al., *Immunological properties of mesenchymal stem cells and clinical implications.* Archivum immunologiae et therapiae experimentalis, 2008. **56**(1): p. 1-8.

148. Tomihata, K. and Y. Ikada, *In vitro and in vivo degradation of films of chitin and its deacetylated derivatives.* Biomaterials, 1997. **18**(7): p. 567-575.